AD-A089 097 HARRY DIAMOND LABS ADELPHI MD F/G 9/1
RESEARCH STUDY ON NEAR MILLIMETER WAVE OROTRONS.(U)
JUL 80 D E WORTMAN, R P LEAVITT
UNCLASSIFIED HDL-SR-80-4 NL

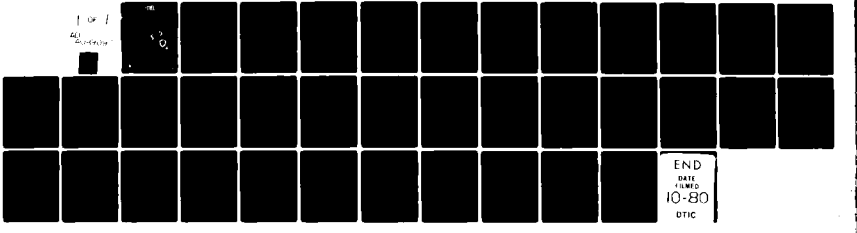

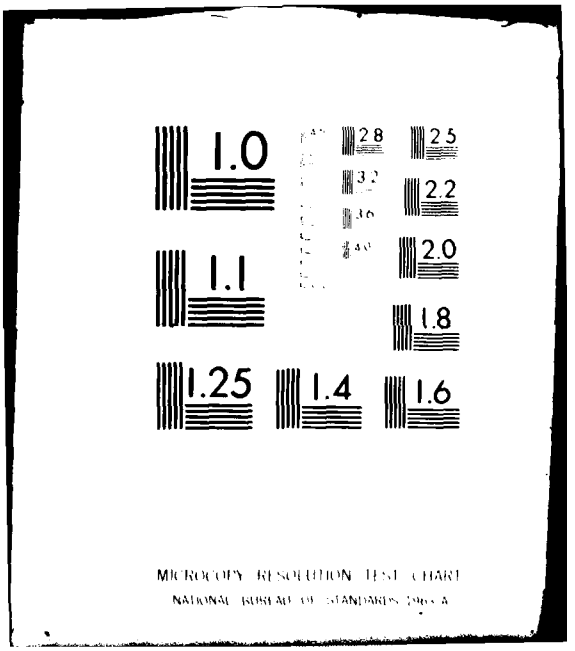
1.0
1.1
1.25
1.4
1.6
1.8
2.0
2.2
2.5
2.8
3.2
3.6
4.0
MICROCOPY RESOLUTION TEST CHART
NATIONAL BUREAU OF STANDARDS 1963-A

# Research Study on Near Millimeter Wave Devices

by Donald E. Thomas
Robert P. Leavitt



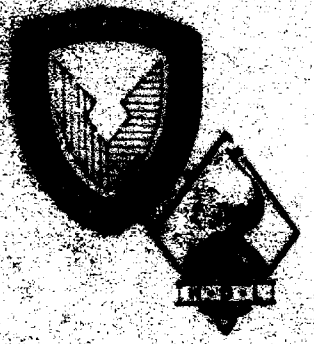

U.S. Army Electronics Research
and Development Command
Harry Diamond Laboratories
Adelphi, MD 20783

UNCLASSIFIED

SECURITY CLASSIFICATION OF THIS PAGE (When Data Entered)

## REPORT DOCUMENTATION PAGE

READ INSTRUCTIONS BEFORE COMPLETING FORM

| | |
|---|---|
| 1. REPORT NUMBER: HDL-SR-80-4 | 2. GOVT ACCESSION NO.: AD-A088697 |
| 3. RECIPIENT'S CATALOG NUMBER | |
| 4. TITLE (and Subtitle): Research Study on Near Millimeter Wave Orotrons | 5. TYPE OF REPORT & PERIOD COVERED: Special Report |
| | 6. PERFORMING ORG. REPORT NUMBER |
| 7. AUTHOR(s): Donald E. Wortman, Richard P. Leavitt | 8. CONTRACT OR GRANT NUMBER(s): DA Project: 1L161102AH44 |
| 9. PERFORMING ORGANIZATION NAME AND ADDRESS: Harry Diamond Laboratories, 2800 Powder Mill Road, Adelphi, MD 20783 | 10. PROGRAM ELEMENT, PROJECT, TASK AREA & WORK UNIT NUMBERS: Program Ele: 61102A |
| 11. CONTROLLING OFFICE NAME AND ADDRESS: U.S. Army Materiel Development and Readiness Command, Alexandria, VA 22333 | 12. REPORT DATE: July 1980 |
| | 13. NUMBER OF PAGES: 37 |
| 14. MONITORING AGENCY NAME & ADDRESS (If different from Controlling Office) | 15. SECURITY CLASS. (of this report): UNCLASSIFIED |
| | 15a. DECLASSIFICATION/DOWNGRADING SCHEDULE |

16. DISTRIBUTION STATEMENT (of this Report)

Approved for public release; distribution unlimited.

17. DISTRIBUTION STATEMENT (of the abstract entered in Block 20, if different from Report)

18. SUPPLEMENTARY NOTES

DRCMS Code: 611102H440011
HDL Project: A44938

19. KEY WORDS (Continue on reverse side if necessary and identify by block number)

Near millimeter waves
Coherent radiation
Submillimeter waves
Microwave tubes

20. ABSTRACT (Continue on reverse side if necessary and identify by block number)

An extensive literature search has been performed in technological areas related to the development of orotrons (electron-beam/open-resonator radiation sources) in the Soviet Union. Orotrons have been found to be practical, tunable, efficient, and lightweight sources of near millimeter wave radiation; our calculations have confirmed some of the conclusions obtained from the Soviet literature. No work on orotrons performed in the U.S. has been found. In work reported from the Soviet Union, power outputs of several watts have been obtained at wavelengths from 4 to 1 mm, with electron-beam voltages of 1 to 5 kV and currents up to a few hundred milliamperes.

DD FORM 1 JAN 73 1473 EDITION OF 1 NOV 65 IS OBSOLETE

UNCLASSIFIED

1 SECURITY CLASSIFICATION OF THIS PAGE (When Data Entered)

163050

## CONTENTS



## FIGURES

## CONTENTS (cont'd)



## TABLES

# 1. INTRODUCTION

Conventional sources of electromagnetic radiation in the microwave region (klystrons, magnetrons, traveling wave tubes, etc) become extremely inefficient as the wavelength of radiation approaches the submillimeter range [1].* This is so both because of fundamental frequency limitations on these devices and also because manufacturing tolerances become too stringent. Approaching the near-millimeter-wave (NMMW) range from the other end of the spectrum, the optical, presents difficulties in that the efficiencies in these devices (optically pumped lasers) are restricted by the Manley-Rowe condition [2]. These restrictions have required the development of new devices which are intended primarily for the production of NMMW radiation.

Much theoretical [3-7] and experimental work [8-10] has been performed in attempting to produce NMMW radiation via the Cerenkov effect. Microwave Cerenkov radiation was first detected at a wavelength of 1.25 cm by Danos et al [8]. Recently [10], 1 MW of radiation at a wavelength $\lambda = 4$ mm was produced by the passing of an electron beam through the center of a hollow dielectric tube. Thus, the Cerenkov effect appears to be a reliable method of producing NMMW radiation, although practical devices based on this effect have yet to be developed. Other new effects and devices which show some promise in the NMMW area include the free electron laser [11-14] and the upshifting [15] of microwave radiation by an electron beam in a medium (SESR — stimulated electromagnetic shock radiation).

Of all the new effects proposed to produce NMMW radiation, only two have been developed into laboratory operating devices: the gyrotron [16, 17] and the orotron. The orotron is based on the Smith-Purcell effect [18], which was first suggested by Frank [19]. Smith-Purcell radiation is produced when an electron beam skims the surface of a metallic diffraction grating. In general, radiation produced when charged particles pass close to, but do not touch, metallic objects is known as diffraction radiation. We shall consider as orotrons all devices that make use of diffraction radiation or the Smith-Purcell effect, together with an open resonator for feedback.

The first orotrons were developed independently by Rusin et al in the Soviet Union [20] and by Mizuno et al in Japan (that group called the device the ledatron [21] ). These devices consisted of an electron beam passing over a diffraction grating which, together with another reflecting surface, formed an open resonator (see fig. 1). The Soviet version had a spherical smooth mirror, whereas the Japanese had a plane smooth mirror. The Japanese [22] discussed two distinct modes of operation of their device, one corresponding to the mode observed in the Soviet orotron, and the other corresponding to the backward-wave mode observed in backward-wave oscillators. The separation of mirrors was 1 to 2 mm in the Japanese work, and 20 to 30 mm in the Soviet work. Nevertheless, the devices discussed were for all practical purposes identical, and we shall refer to them both as orotrons.

Some of the attractive features that emerged from these early studies were a high degree of tunability (up to a factor of two in output frequency), compactness, and a high stability (because of the high-Q open resonators). However, output powers, $P_{out}$, and efficiencies reported in these studies were disappointingly low, and the electron beam currents, $I_s$, necessary to obtain oscillation were extremely high. Typical figures [22] are $P_{out} = 300$ mW, $I_s = 800$ mA, for an overall efficiency of 0.0025 percent. Characteristics such as these are what produced the original negative reactions to the orotrons in the U.S.

Later work in the Soviet Union, summarized in the book by Shestopalov [23], showed that, with improvement in resonator design, the efficiencies of these devices could be improved by more than three orders of magnitude. In the orotrons discussed by Shestopalov, typical output powers of several watts could be produced with starting currents of 25 to 50 mA, with efficiencies of 1 to 2

* *Because of the nature of the literature survey, the references in this report are too extensive to be listed on each page. The numbers in brackets refer, therefore, to the Literature Cited, at the end of the report.*

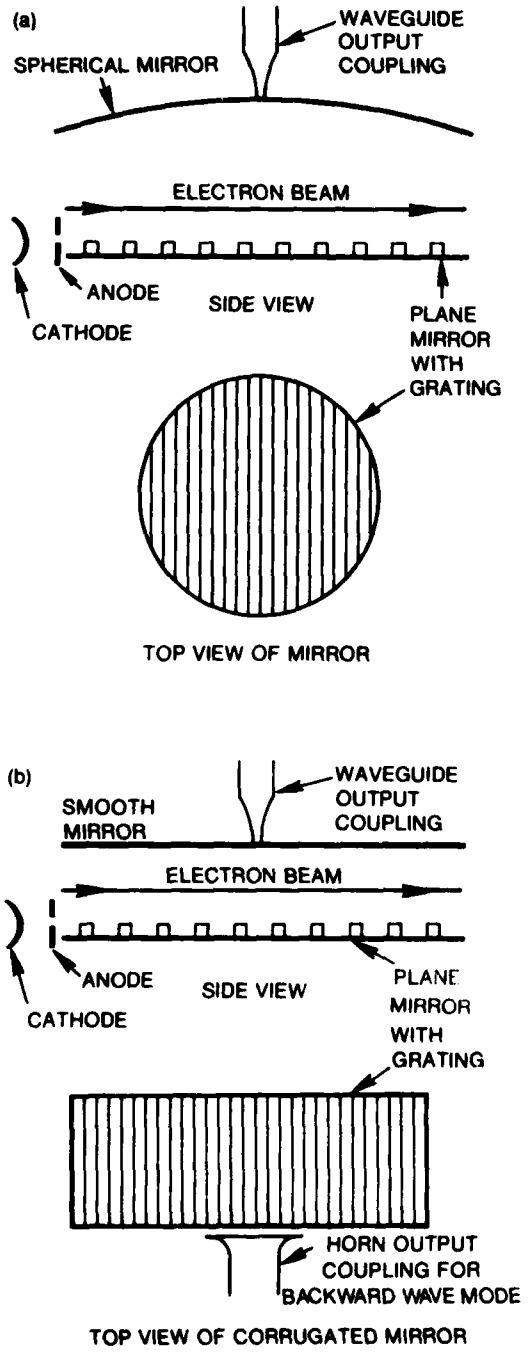


**Figure 1. First-generation orotrons: (a) Rusin's orotron and (b) Mizuno's ledatron.**

percent. The main difference between these devices (called DRG's by Shestopalov, or diffraction radiation generators) and earlier devices is that the newer devices used a strip grating (fig. 2) partially covering the plane mirror, whereas in the earlier orotrons the grating completely covered the plane mirror. It is with this latter generation of orotrons that we have been primarily concerned in this study.

We have found that the orotron is a practical source of NMMW radiation. Our findings are discussed in this report; for each technological area connected with orotron research, we summarize the state of the art and make recommendations for further research. In section 2 we discuss the basic theory of operation of the orotron; the mechanism of electron bunching in particular is found to be important in analyzing orotron behavior. In section 3 the characteristics of diffraction gratings in

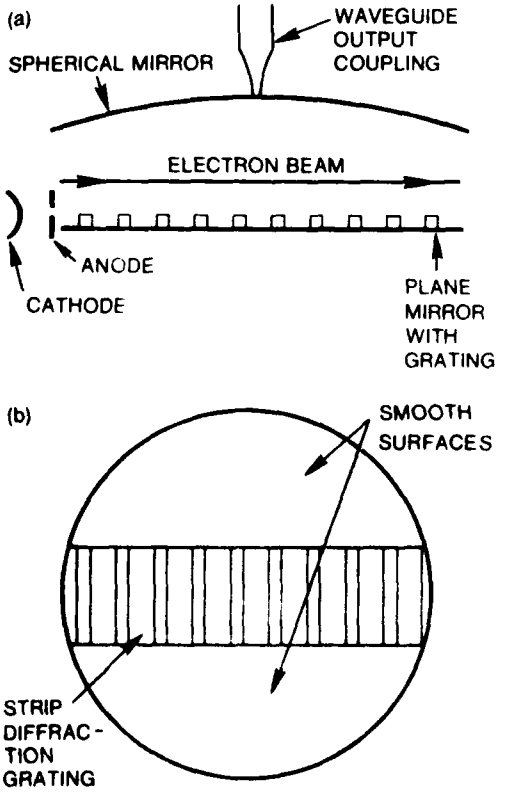


**Figure 2. Shestopalov's DRG (diffraction radiation generator).**

orotrons are discussed; the theory of Smith-Purcell radiation is used to determine optimum grating dimensions for orotrons. Experimental studies on the effects of various grating parameters on the operation of orotrons are reviewed. Section 4 discusses resonator theory and gives a review of resonators that have been used or proposed for use in orotron systems. Section 5 discusses various output schemes that have been devised or suggested. Section 6 discusses the theory of electron guns, and suggests some possible designs for use in orotrons.

## 2. THEORY OF OPERATION OF THE OROTRON

A new type of electron tube has evolved over the last two decades, called the orotron [20], ledatron [21], or diffraction radiation generator [23]. The tube, basically, consists of an electron beam generator and collector and a Fabry-Perot cavity containing one grooved mirror (grating) and one smooth mirror. The principle of operation of the orotron is based on the Smith-Purcell effect [18].

### *2.1 Theory of the Smith-Purcell Effect*

Consider a metallic grating of period $\ell$ over which an electron beam of velocity $v_0$ is passed, as shown in figure 3. As the electrons move over the grating, they induce image charges in the grating which move up and down the grooves of the grating. The image charges also act back on the electrons in the beam to accelerate them. This system of accelerating charges radiates according to Maxwell's theory. The Smith-Purcell effect may also be viewed as diffraction of the electromagnetic field of the electrons by the grating (diffraction radiation). We may consider a frequency decomposition of the electromagnetic fields, and thus work at a frequency $\omega$.

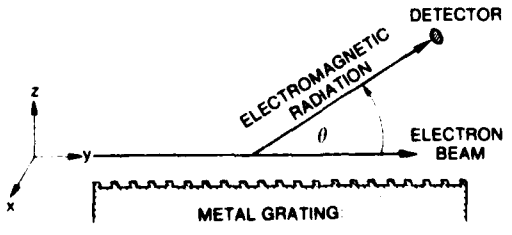


**Figure 3. Basic Smith-Purcell experiment.**

Consider a model in which the beam and the grating have infinite extent, both out of the paper (x-direction) in figure 3 and to the left and right (y-direction). Let the z-direction be normal to the grating surface. Then the electromagnetic field is a transverse magnetic (TM) field, and we may consider the x-component of the magnetic induction $H_x$, alone. Because of the periodic boundary conditions at the grating surface, $H_x$ takes the form

$$H_x = e^{-i\omega t} \sum_{m=-\infty}^{\infty} H_m(z)\, e^{i(\alpha + 2\pi m/\ell)y} \quad , (1)$$

where t is time and the functions $H_m(z)$ describe the z-dependence of the mth-order mode. In particular, in the free-space region above the electron beam, we have

$$H_m(z) = H_m(0)\, e^{-\Gamma_m z} \quad , \qquad (2)$$

where $\Gamma_m = \sqrt{(\alpha + 2\pi m/\ell)^2 - (\omega/c)^2}$. The coefficients $H_m(0)$ depend on the detailed nature of the grating and the electron beam. The coefficient $\alpha$ is determined by requiring that the phase velocity of the zero-order field $H_0$ be equal to the electron beam velocity; therefore

$$\alpha = \omega/v_0 \quad . \qquad (3)$$

The phase velocity of the mth mode is given by

$$v_p(m) = \frac{\omega}{\alpha + 2\pi m/\ell} \quad . \qquad (4)$$

It can be seen from equation (2) that those modes with $|v_p(m)| < c$ do not radiate, whereas those with $|v_p(m)| > c$ radiate. This condition restricts the radiating modes to a finite number.

For those modes that radiate, the angle of radiation, $\theta$, is related to the frequency by

$$\cos\theta = \frac{c(\alpha + 2\pi m/\ell)}{\omega} \qquad (5)$$

Using equation (3) in (5) and expressing the frequency in terms of the wavelength $\lambda = 2\pi c/\omega$, we obtain

$$-m\lambda = \ell\,(c/v - \cos\theta) \qquad (6)$$

This is the Smith-Purcell formula.

The determination of the coefficients $H_m(0)$ in equation (2) is a tedious electromagnetic boundary value problem that has attracted the attention of a number of authors [24-29]. The main results of these calculations may be summarized as follows.

1. The beam-grating interaction is relatively weak and decreases exponentially as the beam-grating distance is increased.
2. The interaction of the grating back on the beam to cause bunching is weak.
3. The radiated power is spread over 180 deg in angle and is over a wide range of frequencies.

The first attempt at using the Smith-Purcell effect in a practical radiation device was the varotron [30], which essentially consists of the Smith-Purcell experiment with a high-current electron beam. Because of the large spread in frequency and angle noted above, the device operated essentially as an electron-beam pumped light bulb; i.e., a broadband noise source.

Improved efforts at constructing a coherent NMMW source using the Smith-Purcell effect were initiated by the Russians [20] and Japanese [21]. The devices that these researchers produced (called, respectively, the orotron and ledatron) consist of the Smith-Purcell experiment placed in a Fabry-Perot resonator with the grating acting as one of the resonator mirrors, as shown in figure 1. The purpose of the resonator is to select a particular frequency out of the Smith-Purcell radiation and feed it back on the electron beam, thus causing bunching of the beam.

Another way of viewing these orotrons is to consider [21] the Fabry-Perot resonator with one grooved mirror to be a resonator capable of supporting both slow and fast waves; the electron beam interacts with the slow waves, and the resonator supports the resultant fast waves. Mizuno [22] found two different modes of operation of the ledatron, but the second mode (a backward-wave mode) may, for the purposes of NMMW generation, be regarded as spurious since it is inefficient and it operates at a longer wavelength than the other (Fabry-Perot) mode.

The wavelength of operation of the Fabry-Perot mode is determined from equation (6), since only that radiation emitted at 90 deg is resonant with the cavity. Therefore, assuming that the fundamental mode ($m = -1$) dominates, we get

$$\lambda = \frac{\ell c}{v} \qquad (7)$$

This relation is found to hold experimentally. Figure 4 shows the operating curves of orotrons (wavelength versus beam accelerating voltage) for various values of $\ell$ appropriate for the NMMW region.

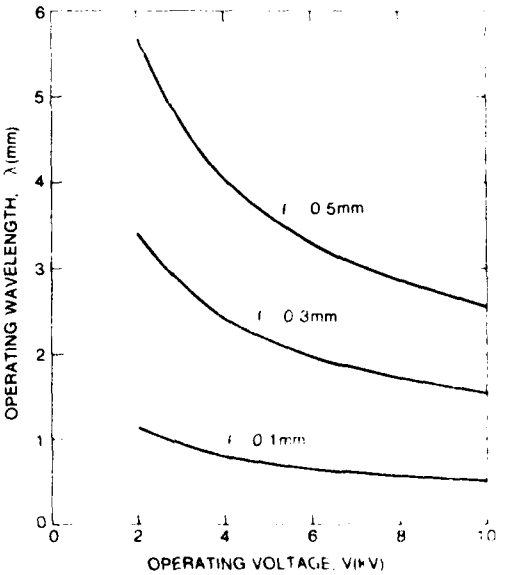


**Figure 4. Operating characteristics of orotrons.**

## 2.2 *Electron Bunching in Orotrons*

Although the Smith-Purcell effect is the mechanism underlying orotron operation, it is the bunching of the electrons in the beam that allows coherent radiation by the device. Determining the operational conditions for orotrons requires analyzing this bunching in detail. We shall consider a simple idealized model.

Consider the simple model depicted in figure 5. We assume an rf electric field in the orotron resonator along the y-axis, whose magnitude at the nth groove of the diffraction grating is $E_n(x)\, e^{-i\omega t}$, where $\omega$ is the frequency of the rf field. The electric field is assumed to be zero between grooves (this is so because of the boundary condition on the tangential component of the field at the grating). Let $\ell$ be the grating period, and d the groove width. Consider an electron in the beam whose velocity is $v_n$ when it arrives at the nth groove. Let its time of arrival at the nth groove be $t_n$. Upon reaching the groove, the electron will be accelerated or decelerated by the rf field, depending on the phase of the field at its time of arrival. After traversing the groove, the velocity of the electron is found to be

$$v_{n+1} = v_n - \frac{ieE_n}{\omega}\left[e^{-i\omega t_n'} - e^{-i\omega t_n}\right] , \qquad (8)$$

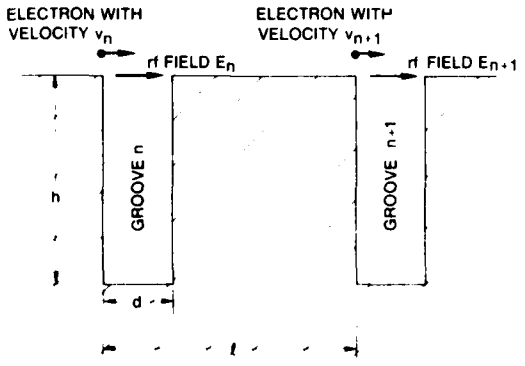


**Figure 5. Electron bunching in orotrons.**

where $t_n'$ is the time of arrival of the electron at the end of the groove. The quantity $t_n'$ is determined by

$$d = v(t_n' - t_n) + \frac{eE_n}{\omega^2}\left[e^{-i\omega t_n'} - e^{-i\omega t_n}\right] + \frac{ieE_n}{\omega}(t_n' - t_n)\, e^{-i\omega t_n} . \qquad (9)$$

Having arrived at the end of groove n at time $t_n$, the electron then travels to groove $n + 1$ with velocity $v_{n+1}$, thus

$$\ell - d = v_{n+1}(t_{n+1} - t_n') . \qquad (10)$$

The above three equations determine $v_{n+1}$, $t_n'$, and $t_{n+1}$, in terms of $v_n$ and $t_n$, and thus may be iterated to determine the motion of an electron over the entire grating surface. However, the equations as they stand are not amenable to closed-form solutions, as they require numerical solution at each iteration.

This difficulty may be eliminated if we perform a small signal analysis; that is, we assume the rf field to be small enough so that the equations may be linearized. This allows us to compute the current density in the beam in closed form. From the current density we may obtain the power radiated by the beam according to Poynting's theorem as

$$P_{rad} = -\frac{1}{2}\,\mathrm{Re}\int \vec{J}\cdot\vec{E}^{*}\, dV , \qquad (11)$$

where the integral is over the volume occupied by the electron beam, and where $\vec{J}$ is the rf component of the current density ( * = complex conjugate).

The grating-beam system, of course, is immersed in a cavity which supports the rf electric field $\vec{E}$. The total energy in the cavity is

$$U = \frac{1}{4}\,\mathrm{Re}\int\left(\varepsilon_0|\vec{E}|^2 + \mu_0|\vec{H}|^2\right) dV' , \qquad (12)$$

where the integral extends over the resonator volume. In the above, H is the rf magnetic field in the cavity, $\varepsilon_0 = 8.854 \times 10^{-12}$ F/m is the vacuum permittivity, and $\mu_0 = 4\pi \times 10^{-7}$ H/m is the vacuum permeability. A radiative Q for the cavity may be defined as (see sect. 4)

$$Q_{rad} = -\frac{\omega U}{P_{rad}} \qquad (13)$$

(being negative, since the radiation increases the stored energy), and the starting current for coherent radiation is determined by the condition

$$\frac{1}{Q_0} + \frac{1}{Q_{rad}} = 0 \quad , \qquad (14)$$

where $Q_0$ is the quality factor of the resonator. This condition gives for the starting current

$$\frac{1}{I_{start}} = \frac{-e\,Q_0}{m\omega^3\varepsilon_0}\,\mathrm{Re}\sum_{n=1}^{N}\sum_{k=1}^{n-1} \times f_n^* f_k\, e^{i\omega(n-k)\ell/v_0}$$

$$\times\left[4\left(1-\cos\frac{\omega d}{v_0}\right)-2\,\frac{\omega d}{v_0}\sin\frac{\omega d}{v_0}\right.$$

$$\left.-2\,\frac{i\omega\ell}{v_0}(n-k)\left(1-\cos\frac{\omega d}{v_0}\right)\right]$$

$$+\frac{i\omega d}{v_0}\left(e^{\frac{i\omega d}{v_0}}-1\right)|f_n|^2 \quad , \qquad (15)$$

where N is the total number of grooves, and

$$f_n^* f_k = \frac{1}{B}\int_{-B/2}^{B/2} E_n^*(x)\,E_k(x)\,dx \quad , \qquad (16)$$

where the integral is over the width B of the electron beam. The quantity $E_n(x)$ is the field at the nth grating groove as a function of the transverse coordinate x, such that the energy (12) is normalized to unity over the resonator volume. The quantity $v_0$ is the initial electron velocity, given by

$$v_0 = \sqrt{\frac{2eV}{m}} \quad , \qquad (17)$$

where V is the beam accelerating voltage.

In evaluating the above expression for actual orotrons, one must use the resonator modes given in section 4; in this case the dependence of $f_n$ on n is Gaussian. We have evaluated starting currents from equation (15); the starting current is found to be strongly dependent on the parameter

$$\theta = \frac{\omega\ell}{v_0} \quad , \qquad (18)$$

which is found to be $2\pi$, from the theory of the Smith-Purcell effect. In actuality, from equation (15) we find $\theta$ somewhat less than $2\pi$. To choose a concrete example, we choose a resonator whose mirror spacing is 25 mm. The grating is assumed to have a length of 40 mm and a width of 10 mm. The groove spacing of the grating is 0.4 mm and the groove width is 0.15 mm (these values are found to be optimum for radiation at $\lambda = 4$ mm; see sect. 3). The spot sizes along x and y (see sect. 4) are both chosen to be 10 mm. We choose a resonator Q of 5000, typical of those obtained experimentally (sect. 4).

Figure 6 shows the starting current for the above parameters as a function of the phase angle $\theta$. The phase angle at which the orotron operates corresponds to the minimum in the figure, or

$$\frac{\omega\ell}{v_0} = 6.248 \quad .$$

This gives, for $\lambda = 4$ mm operating wavelength, $v_0 = 3.02 \times 10^7$ m/s for an accelerating voltage V = 2590 V. The starting current for these conditions, from figure 6, is 11 mA, about a factor of two lower than that observed experimentally (see sect. 4).

As can be seen, the electron bunching theory provides a good estimate of operating conditions; however, the theory is still in crude form; improvements need to be made so that the theory can guide the design of orotrons operating at smaller wavelengths.

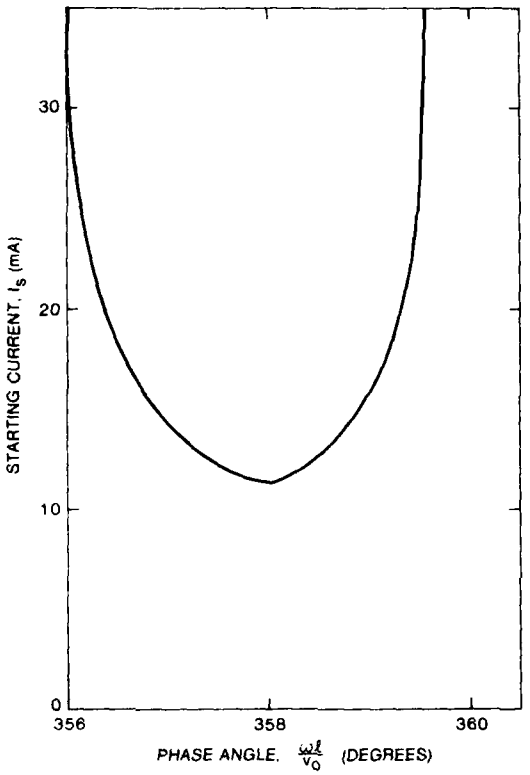


**Figure 6. Dependence of starting current on phase angle.**

## 3. OROTRON DIFFRACTION GRATINGS

The diffraction gratings used in the orotron are an integral part of the resonant cavity. Consequently, in designing a grating that will give maximum performance, the interaction of the electron beam with the grating positioned in the cavity has to be considered. Theoretical analysis of this problem is quite complex, and so experimental investigation has been the main method for these studies. A vast amount of experimental information has been published [23] concerning the effect of the diffraction grating on the operation of orotrons, and we will use this information primarily for designing appropriate gratings for proposed experiments for an orotron that works in the 4-mm wavelength range.

As far as the theoretical treatment of the problem is concerned, the topic of electron beams interacting with gratings and other periodic structures is too vast to be covered here. We will not attempt to list all the contributors to the field; however, we will give results from several of the papers that develop the theory for determining optimum grating parameters. Much of the theory for different types of gratings is given by Shestopalov [23]. Various other papers are also useful [24, 26, 27, 29, 31-37]. Some of the physical results which have been determined for periodic strip-type gratings are particularly useful. These solutions make it possible to compare theoretical results for more complex situations and to give guidance for setting up experiments intelligently.

### *3.1 Theoretical Predictions*

The emission from charged particles passing over periodically repeated inhomogeneities shows certain specific characteristics. Some of these characteristics were discussed in section 2. There we supposed that a modulated electron beam passes close to a flat diffraction grating as shown in figure 3. The emission spectrum is determined only by the period of the grating, and equation (6) gives the relation of the emission frequency to the velocity of the source. The emission spectrograms obtained by Smith and Purcell verified these formulas. In the case of a periodic strip-grating, where d is the strip width and $\ell$ is the period as shown in figure 7, Shestopalov [23] determined the optimal value of d at which radiation is a maximum in the interval $0 < d < \ell$. He showed that when a wave is radiated in the direction of the normal to the grating, the optimal value, $d_{opt}$, is obtained approximately by the formula

$$d_{opt} \approx \ell \frac{2}{\pi} \sin^{-1} \sqrt{\zeta \left(1 + \frac{\zeta^2}{\zeta^2 - \chi^2}\right)} \quad , \quad (19)$$

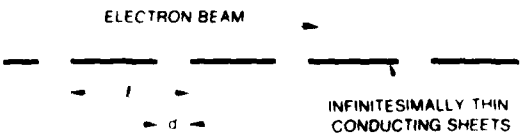


**Figure 7. Strip grating.**

under the condition that $\left|\frac{\zeta^2}{\zeta^2 - \chi^2}\right|^2 << 1$.

Here $\zeta$ is the solution of the transcendental equation

$$e^{-\zeta/\chi^2} = \zeta \quad , \tag{20}$$

and $\chi = \ell/\lambda$.

Since actual gratings to be used in orotrons can have different shapes, it is necessary to compare different grating configurations. Shestopalov [23, pp 52-63], carries out a comparative analysis of periodic structures for determining the optimal profile of any grating which should be selected for a particular type of generator where the Smith-Purcell effect is used for generating oscillations. This comparative analysis determines the configuration that maximizes the amplitude of the plane wave that is radiated away from the grating during the passage of the electron stream above it. The most acceptable profile is also selected according to the possibility of operating the generator at higher space harmonics. This consideration may be advantageous for creating orotrons that operate in the submillimeter wavelength range.

The types of reflection gratings considered by Shestopalov are shown in figure 8. These he calls (a) a comb type, (b) an echelette with rectangular teeth, and (c) gratings of circular semicylinders lying on a metallic plane. Shestopalov found the energy characteristics of Smith-Purcell radiation for each grating by generating the appropriate equations for the diffraction of a nonhomogeneous plane wave on the gratings, which he then solved by numerical computation on a computer.

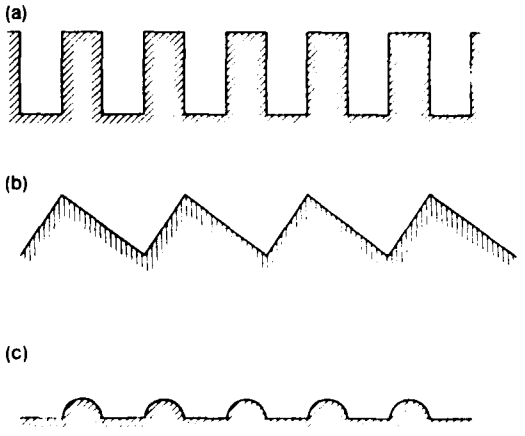


**Figure 8. Gratings considered in Smith-Purcell radiation: (a) rectangular bars, (b) echelette, and (c) semicircular cylinders.**

From these extensive numerical calculations, it was found [23, p 58] that only the comb has sufficient vertical radiation to be of interest in the type of orotron described here. For the echelette and the grating of semicylinders, vertical radiation is extremely small; and although lateral radiation is intensive, it is directed at very small angles in relation to the grating.

The numerical calculations described above also show that the energy maxima of the radiated harmonics occur when the comb depth is $h \approx 0.22\lambda$. Using this comb depth, Shestopalov obtained the optimum value of $\theta = d/\ell$ for the comb [23, p 50]. For maximum radiation coming off normal to the grating,

$$|\Delta h| = \lambda \frac{\theta}{2\pi} \quad . \tag{21}$$

This limitation is used to determine the tolerances for the manufacture of the gratings.

### *3.2 Experimental Studies*

The theoretical studies described above suggest that comb-shaped grating (rectangular grooves in a metal surface) be used; they also give grating parameters that optimize the energy coming away from the grating. Extensive experimental work has confirmed these theoretical results and has shown how certain other factors (such as grating length, width, and edge effects) affect the performance of the orotron. These experimental results also indicate how the grating should be positioned within the cavity for cavities of different shapes.

It was found [23, p 180] that the resonator mirror that is partially covered (as opposed to

completely covered) by a diffraction grating has a more rarefied oscillation spectrum. By changing the width of the grating, one can change substantially the number of types of oscillations excited in the open resonator and control the distances at which oscillations of a higher order may appear. In order to improve the output characteristics of the ortron, it is then essential to determine the effects of the finite dimensions of the reflecting diffraction grating and the various inhomogeneities on it. Shestopalov [23] gives results of such studies.

First, Shestopalov discusses the effect of the grating edges on the operation of the orotron. Surface waves are generated in the orotron whose reflections either enhance or degrade the rf electric field interacting with the electron beam. Thus, in general, the operating conditions of the orotron become somewhat frequency sensitive. In an attempt to remedy this situation, Shestopalov systematically studied the effect of the ends of the grating on the generator's operation on a specially manufactured orotron designed to operate at a wavelength $\lambda = 4$ mm. Some of the results are summarized in table 1. This study shows that the greatest variation of output power with frequency is characteristic of reflecting diffraction gratings with grooves of equal depth over the entire length from the anode to the collector. There is a weaker dependence of the output power on the frequency in an orotron whose grating has flat pedestals 4 mm long near the gun and collector ends of the grating. For the gratings in which the depth of the grooves on the 10 extreme periods was increased or reduced, a more uniform variation in the level of the output power over the tuning range was observed.

In the above cases, resonance with respect to a slow wave was observed, which was caused (regardless of the way the reflecting diffraction grating was prepared) by the nonremovable reflection of the surface from the ends of the grating (the value of the reflection factor and its phase depend on the frequency and geometry of the ends of the grating). Total removal of reflection from the ends of the grating is achieved by covering the extreme grooves with aquadag or by filling them with graphite plates. For gratings with ends covered with aquadag, the output power changes more smoothly with the changes in their frequency than in all preceding cases. The insufficient absorbing ability of a thin layer of aquadag resulted in the reflection of the surface wave from the ends of the grating at frequencies of 59 and 65 GHz in an unfavorable phase, and at 57 and 63 GHz in a favorable phase, which changed the level of the output power at these frequencies. By using graphite plates instead of aquadag, it was possible to achieve orotron excitation with a power which changed relatively little over almost the entire tuning range.

**TABLE 1. EFFECT OF GRATING END TERMINATION ON OROTRON PERFORMANCE**

| Method of making extreme slots in diffraction grating | Minimum starting current (mA) | Output power (W) | Tuning range (%) |
|---|---|---|---|
| Ordinary grating | 70 | 0.7 | 13 |
| No slots at end of grating | 50 | 0.6 | 20 |
| Smooth deepening of extreme 10 slots from 0.98 to 1.2 mm | 45 | 0.6 | 23 |
| Smooth decrease of extreme 10 slots from 0.98 to 0.78 mm | 60 | 1.3 | 24 |
| Ends of grating covered with aquadag | 40 | 0.5 | 20 |
| Graphite inserts in ends of grating | 70 | 0.75 | 17 |

The shape of the ends of the reflecting diffraction grating also influences the starting currents and the tuning range (table 1). The tuning range is minimal in an orotron with a grating in which the grooves have the same depth along the entire length (there is no matching with respect to the surface wave). The tuning range widens for a grating with flat pedestals at the ends. It is widest when the depth of the grooves decreases smoothly at the 10 extreme periods (the widening of the tuning band in this orotron was obtained at the expense of the high-frequency part of the tuning range). The highest efficiency, a wide tuning range, and a relatively smooth change in the starting currents and output power were achieved in the gratings with smooth deepening of the 10 extreme slots by 0.05 mm every two periods.

Shestopalov [23] also reported results of experimental work to determine optimal grating widths. For example, at $\lambda = 4$ mm, optimal data were obtained for grating widths of 10 to 15 mm; when the grating was widened further, the excitation conditions of the resonator worsened, since there was some increase in the ohmic losses (they are proportional to the area occupied by the grating) and diffraction losses (occurring when the field spot does not correspond to the width of the grating). When the reflecting grating is widened, the excitation conditions of the orotron worsen also, because the directional pattern of diffraction radiation does not correspond to the excited type of oscillations of the resonator.

Experiments were also performed to determine the optimum length of the reflecting diffraction grating. The experiments show [23, p 299] that for normal operation of the orotron, the grating length must be more than twice as long as the dimensions of the field caustic (see sect. 4), since, in spite of the smallness of the field beyond the caustic, the preliminary modulation of the electron stream has a substantial effect on the operation of the generator. This phenomenon can be explained clearly by means of the theory of electron bunching, which we discussed earlier.

In orotrons which use a plane mirror in the open resonator, the position of the grating surface with respect to the mirror surface is important. For example, in the case of an orotron with the top surface of the reflecting diffraction grating applied flush with the plane mirror, the effective excitation of oscillation takes place in those regions and on those types of oscillations where the effect of the grating is relatively small: in this case, there is a field minimum at the grating-mirror boundary. The excitation conditions for oscillations with different field distributions result in an increase in the starting current and a decrease in the level of the output power.

In the orotron in which the effect of the grating raised above the surface of the plane mirror was reduced to a minimum, the excitation conditions for the same type of oscillation were practically identical over the entire tuning range. This was revealed by the dependence of the starting current on the wavelength for several types of oscillations. For the orotron with the elevated grating, the starting currents changed smoothly not only within the limits of one oscillation, but over the entire range. The power changed in the same way depending on the wavelength. The optimum height of the grating surface above the plane mirror surface was found to be 0.6 mm, for $\lambda = 4$ mm. It was found that the position of the grating does not adversely affect the orotron operation for certain other cavities such as a spherocylindrical cavity; this is discussed further by Shestopalov [23].

For example, the theoretical and experimental results published by the Soviets [23] give detailed information required for the proper selection of an orotron grating. The theoretical calculations give the optimum grating parameters that relate the wavelength, groove pitch, groove width and depth, and the beam's electron velocity. The experimental results show the importance of the position of the diffraction grating surface with respect to the mirror surface for one particular cavity configuration. Edge effects caused by the finite size of the grating elements were also explored in detail. The optimum conditions for the length and width of the grating were also examined in much detail experimentally.

Following this earlier Soviet work, a grating was constructed as shown in figure 9. The grating material is copper. The grating should have a high conductivity to cut down on ohmic losses. This fact suggests that silver might be desirable, but it would be no better than copper because of other mechanical considerations.

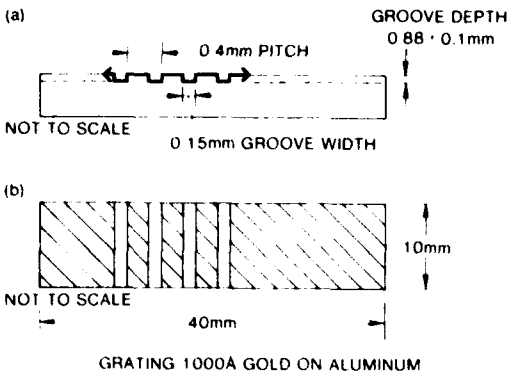


**Figure 9. Recommended diffraction grating.**

## 4. OPEN RESONATORS USED IN OROTRONS

The feature that distinguishes orotrons from other electron tube oscillators and amplifiers is the use of a high-Q open resonator as a feedback device. The open resonator allows the buildup of large electric-field oscillations near the electron beam, which cause the beam to become bunched. This allows the orotron to operate at relatively high efficiency in spite of the fact that the basic radiation mechanism (the Smith-Purcell effect) is weak. In the present section we examine the properties of high-Q open resonators and review numerous experimental studies of these resonators.

### *4.1 Theory of Basic Open Resonators*

Of primary interest is the distribution of electromagnetic radiation in the interior of an open resonator. We shall consider resonators whose mirrors are spheroidal. The axis of the resonator is assumed to be along the z-axis. Approximate analytical solutions can be obtained for the resonator modes in this case by writing [38]

$$E(x,y,z) = \psi(x,y,z)\, e^{ikz} \quad , \qquad (22)$$

where E is a transverse component of the electric field and where $k = 2\pi/\lambda$ is the wave vector corresponding to the frequency $\omega = ck$, where c is the speed of light in a vacuum. Assuming that

$$\left| k \frac{\partial \psi}{\partial z} \right| >> \left| \frac{\partial^2 \psi}{\partial z^2} \right| << k^2 \psi \quad ,$$

the wave equation becomes

$$\frac{\partial^2 \psi}{\partial x^2} + \frac{\partial^2 \psi}{\partial y^2} + 2ik \left| \frac{\partial \psi}{\partial z} \right| = 0 \quad . \qquad (23)$$

The above approximation is equivalent to assuming $w >> \lambda$, where w is the tranverse width of the electromagnetic field pattern. We shall find that this condition is not strictly satisfied for the resonators and wavelengths that we shall consider.

Solutions of equation (23) for freely propagating modes have been obtained [39]. These are

$$E_{n,m}(x,y,z) = E_0 \sqrt{\frac{w_{0x} w_{0y}}{w_x(z) w_y(z)}} \times H_n\left[\sqrt{2}\, \frac{x}{w_x(z)}\right] H_m\left[\sqrt{2}\, \frac{y}{w_y(z)}\right] \times \exp\left[ - \frac{x^2}{w_x(z)^2} - \frac{y^2}{w_y(z)^2} + ik \frac{x^2}{2R_x(z)} + ik \frac{y^2}{2R_y(z)} + ikz - i(n + \tfrac{1}{2})\eta_x(z) - i(m + \tfrac{1}{2})\eta_y(z) \right] , \qquad (24)$$

where

$$w_x(z) = w_{0x} \left[ 1 + \left( \frac{z - z_{mx}}{z_{0x}} \right)^2 \right]^{1/2} , \qquad (25)$$

$$R_x(z) = \frac{1}{(z - z_{mx})}\left[(z - z_{mx})^2 + z_{0x}^2\right] , \quad (26)$$

$$\eta_x(z) = \tan^{-1}\left(\frac{z - z_{mx}}{z_{0x}}\right) , \quad (27)$$

$$z_{0x} = \frac{\pi w_{0x}^2}{\lambda} , \quad (28)$$

with similar relations for $w_y(z)$, $R_y(z)$, $\eta_y(z)$, and $z_{0y}$ in terms of $z_{my}$ and $w_{0y}$. In equation (24), the quantities $H_n$ and $H_m$ are Hermite polynomials of degree n and m, respectively [40]. The parameters $z_{mx}$, $z_{my}$, $w_{0x}$, and $w_{0y}$ are arbitrary constants that will be determined later.

Resonator modes are obtained by superimposing opposite traveling-wave solutions of the form of equation (24) and requiring that they vanish at the surface of both resonator mirrors. Consider a resonator formed by placing a spheroidal mirror (mirror 1) — whose radii of curvature are $R_{1x}$ and $R_{1y}$ — at $z = 0$ and another (mirror 2) — whose radii of curvature are $R_{2x}$ and $R_{2y}$ — at $z = L$.* Then the arbitrary constants are determined by the relations

$$R_{1x} = \frac{1}{z_{mx}}\left[z_{mx}^2 + z_{0x}^2\right] , \quad (29)$$

$$R_{2x} = \frac{1}{(L - z_{mx})}\left[(L - z_{mx})^2 + z_{0x}^2\right] , \quad (30)$$

or

$$z_{mx} = \frac{L(R_{2x} - L)}{(R_{2x} + R_{1x} - 2L)} , \quad (31)$$

$$z_{0x} = \left[\frac{L(R_{2x} - L)(R_{1x} - L)(R_{2x} + R_{1x} - L)}{(R_{2x} + R_{1x} - 2L)^2}\right]^{1/2} . \quad (32)$$

The minimum spot size is found to be

$$w_{0x} = \left[\frac{\lambda^2 L(R_{2x} - L)(R_{1x} - L)(R_{2x} + R_{1x} - L)}{\pi^2(R_{2x} + R_{1x} - 2L)^2}\right]^{1/2} . \quad (33)$$

Identical relations are found between the y-subscripted quantities.

Using equations (29) to (33) in (25), the spot sizes in equation (25) may be determined at any point within the resonator. Of particular interest are the spot sizes at the mirrors. At mirror 1,

$$w_x(0) = \left[\frac{\lambda^2 L(R_{2x} - L)R_{1x}^2}{\pi^2(R_{2x} + R_{1x} - L)(R_{1x} - L)}\right]^{1/4} , \quad (34)$$

and at mirror 2,

$$w_x(L) = \left[\frac{\lambda^2 L(R_{1x} - L)R_{2x}^2}{\pi^2(R_{2x} + R_{1x} - L)(R_{2x} - L)}\right]^{1/4} , \quad (35)$$

with similar relations for $w_y(0)$ and $w_y(L)$.

In addition to the above relations, there is another which is obtained by requiring the boundary conditions to be satisfied simultaneously at both mirrors:

$$(n + \tfrac{1}{2})\left|\eta_x(L) - \eta_x(0)\right| + (m + \tfrac{1}{2})\left|\eta_y(L) - \eta_y(0)\right| = kL - q\pi , \quad (36)$$

where q is an integer and $\eta_x$ and $\eta_y$ are given by equation (27). Equation (36) determines allowed

* The sign convention is chosen so that $R_{x,y} > 0$ if the mirrors curve toward the interior of the resonator.

values of $\lambda(= 2\pi/k)$ for given L, or conversely, allowed values of L for given k. We obtain from equation (27)

$$\eta_x(0) = -\tan^{-1}\sqrt{\frac{L(R_{2x} - L)}{(R_{1x} - L)(R_{2x} + R_{1x} - L)}}, \quad (37)$$

$$\eta_x(L) = \tan^{-1}\sqrt{\frac{L(R_{1x} - L)}{(R_{2n} - L)(R_{1x} + R_{2x} - L)}}. \quad (38)$$

Thus, for a given resonator with a given resonator spacing and wavelength, the modes are characterized by three integral indices (mnq), the first two describing the transverse behavior and the last the longitudinal behavior.

We shall be particularly interested in hemispherical and spherocylindrical resonators. A hemispherical resonator has $R_{1x}$, $R_{1y} \rightarrow \infty$ and $R_{2x} = R_{2y} = R$ (fig. 10). From equation (36) we find that modes with (n + m) fixed are degenerate; that is, they have the same k for fixed L and q. On the other hand, the modes for a spherocylindrical resonator are completely nondegenerate. These resonators have $R_{1y} \rightarrow \infty$, $R_{1x} = R_{cyl}$, and $R_{2x} = R_{2y} = R_{sph}$ (fig. 10).

In particular we consider three resonators whose dimensions are appropriate for use in millimeter-wave orotrons. Resonator 1 is spherocylindrical with $R_{cyl} = 80$ mm, $R_{sph} = 110$ mm. Resonator 2 is spherocylindrical with $R_{cyl} = R_{sph} = 110$ mm. Resonator 3 is hemispherical with $R = 80$ mm. We consider the characteristics of these resonators at a wavelength $\lambda = 4$ mm.

Figure 11 shows the beam spot sizes as given by equations (34) and (35) as a function of the mirror separation L. Note that, for the spherocylindrical resonators, the beam spot sizes at the mirrors along the x- and y-directions may be chosen independently, whereas in the hemispherical resonator they are equal for a fixed separation L. Table 2 lists the allowed resonator modes for mirror spacings between 18 and 20 mm for these resonators.

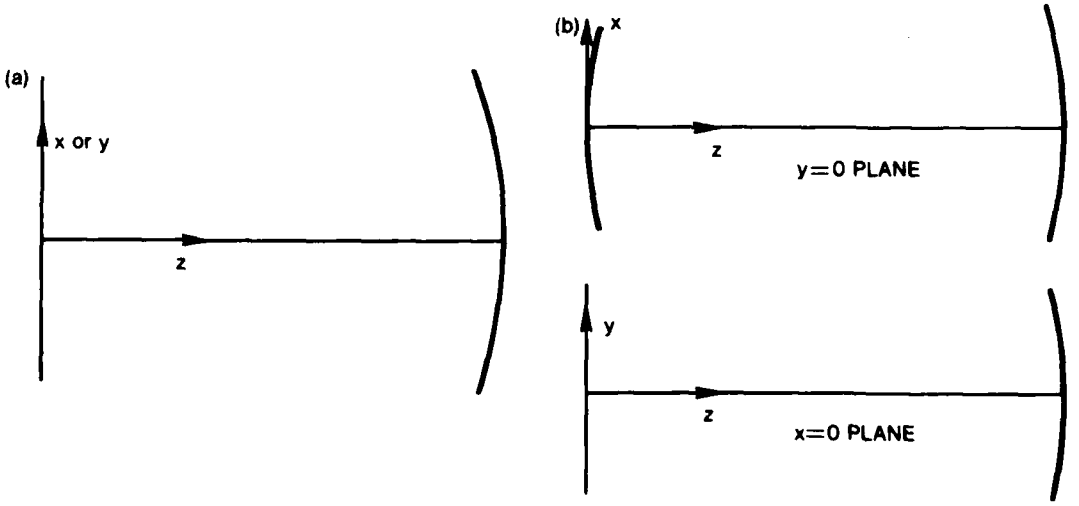


**Figure 10. Resonator configurations: (a) hemispherical and (b) spherocylindrical.**

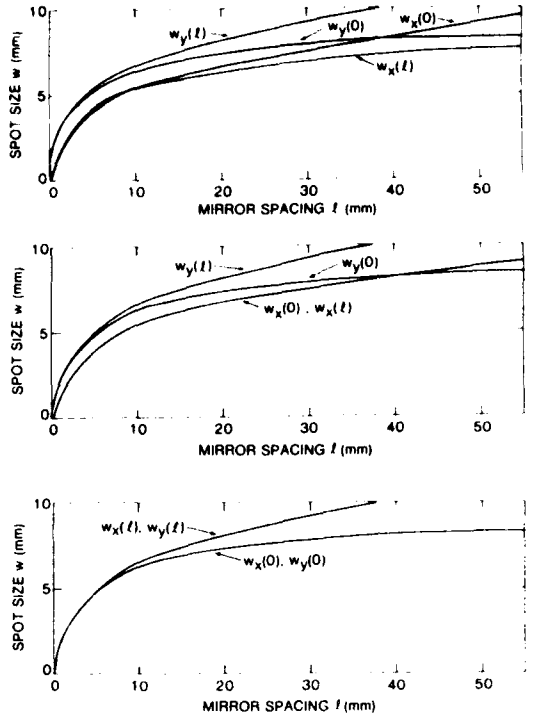


**Figure 11. Spot sizes for various resonators.**

The above considerations are of importance in designing open resonators for use in orotrons. Also of importance are the various loss mechanisms in the resonator. For the orotrons to perform effectively, these losses must be minimized. The quality factor of a resonator is defined by

$$Q = \frac{\omega U}{P} \quad , \tag{39}$$

where U is the stored electromagnetic energy and P is the power dissipated. Losses in the resonators that we are considering are primarily due to four mechanisms:

- ohmic losses at the mirrors,
- diffraction losses,
- scattering losses due to imperfections in mirror construction, and
- output coupling losses.

We consider all these contributions separately below.

Ohmic losses may be calculated through the relation [41]

$$P_{ohm} = \frac{2}{\sigma\delta} \int |\vec{H}_{\parallel}|^2 \, dA \quad , \tag{40}$$

where the integral is over the surfaces of both mirrors, and $\vec{H}_{\parallel}$ is the tangential component of magnetic field at the mirror surface. The quantity $\sigma$ is the conductivity of the mirror material, and $\delta$ is the skin depth, given by

$$\delta = \sqrt{\frac{2}{\mu_0 \sigma \omega}} \quad , \tag{41}$$

where $\mu_0 = 4\pi \times 10^{-7}$ H/m is the vacuum permeability. The electromagnetic energy U stored in the radiation field and occurring in equation (39) may be calculated by

$$U = \tfrac{1}{2} \int (\varepsilon_0 |\vec{E}|^2 + \mu_0 |\vec{H}|^2) \quad , \tag{42}$$

where $\varepsilon_0 = 8.854 \times 10^{-12}$ F/m is the vacuum permittivity and where the integral is over the volume of the resonator. The quantities (40) and (42) may be calculated using the resonator modes corresponding to equation (24). The result is

$$Q_{ohm} = \frac{L}{\delta} \quad . \tag{43}$$

Table 3 gives the skin depth $\delta$ and ohmic Q-factor $Q_{ohm}$ for a few materials of interest at a frequency f = 75 GHz ($\lambda$ = 4 mm) at a resonator spacing of L = 20 mm.

The ohmic Q-factor given by equation (43) is appropriate for resonators bounded by smooth reflectors. In orotrons, however, mirror 1 (the cylindrical mirror in the case of spherocylindrical resonators, the plane mirror in hemispherical resonators) contains a strip grating. The effect of this grating is to severely modify the electromagnetic field distribution near mirror 1 and the

accompanying ohmic losses can become somewhat large. Calculating these ohmic losses is a formidable task, requiring knowledge of the magnetic field at the grating surface (see eq (40)). Calculation of these fields requires the numerical solution of a boundary value problem (see sect. 3); computations of ohmic losses in resonators containing gratings have not yet been performed for this reason. However, experimentally it is found that resonators containing gratings have Q's in the range from 2000 to 6000, indicating that ohmic losses in this case are much more severe than indicated by equation (43).

Computation of diffraction losses in open resonators requires the numerical solution of an integral equation [42], since the solutions (24) are not strictly correct for resonators whose mirrors

**TABLE 2. MODE SPECTRUM OF SOME RESONATORS AT $\lambda$ = 4 mm BETWEEN L = 18 mm AND L = 20 mm[a]**

| Spherocylindrical resonator $R_{cyl}$ = 80 mm, $R_{sph}$ = 110 mm | | | | Spherocylindrical resonator $R_{cyl} = R_{sph}$ = 110 mm | | | | Hemispherical resonator $R_{sph}$ = 110 mm | | | |
|---|---|---|---|---|---|---|---|---|---|---|---|
| n | m | q | L (mm) | n | m | q | L (mm) | n | m | q | L (mm) |
| 1 | 1 | 9 | 18.01 | 2 | 0 | 9 | 18.06 | 0 | 3 | 9 | 18.07 |
| 0 | 3 | 9 | 18.14 | 0 | 3 | 9 | 18.12 | 1 | 2 | 9 | 18.07 |
| 2 | 0 | 9 | 18.15 | 1 | 2 | 9 | 18.23 | 2 | 1 | 9 | 18.07 |
| 1 | 2 | 9 | 18.28 | 2 | 1 | 9 | 18.34 | 3 | 0 | 9 | 18.07 |
| 0 | 4 | 9 | 18.42 | 0 | 4 | 9 | 18.40 | 0 | 4 | 9 | 18.35 |
| 2 | 1 | 9 | 18.43 | 3 | 0 | 9 | 18.44 | 1 | 3 | 9 | 18.35 |
| 1 | 3 | 9 | 18.56 | 1 | 3 | 9 | 18.51 | 2 | 2 | 9 | 18.35 |
| 3 | 0 | 9 | 18.57 | 2 | 2 | 9 | 18.62 | 3 | 1 | 9 | 18.35 |
| 2 | 2 | 9 | 18.71 | 3 | 1 | 9 | 18.73 | 4 | 0 | 9 | 18.35 |
| 3 | 1 | 9 | 18.86 | 4 | 0 | 9 | 18.84 | 0 | 0 | 10 | 19.28 |
| 4 | 0 | 9 | 19.01 | 0 | 0 | 10 | 19.33 | 0 | 1 | 10 | 19.56 |
| 0 | 0 | 10 | 19.35 | 0 | 1 | 10 | 19.61 | 1 | 0 | 10 | 19.56 |
| 0 | 1 | 10 | 19.63 | 1 | 0 | 10 | 19.72 | 0 | 2 | 10 | 19.84 |
| 1 | 0 | 10 | 19.78 | 0 | 2 | 10 | 19.90 | 1 | 1 | 10 | 19.84 |
| 0 | 2 | 10 | 19.92 | 1 | 1 | 10 | 20.01 | 2 | 0 | 10 | 19.84 |

[a] $R_{cyl}$ — radius of curvature of cylindrical mirror
$R_{sph}$ — radius of curvature of spherical mirror
n, m, q — integers from eq (36)
L — length of grating

TABLE 3. SKIN DEPTHS AND OHMIC Q-FACTORS FOR SOME MATERIALS[a]

| Material | $\sigma$ ($\times 10^7$ mho/m) | $\delta$ ($\times 10^{-5}$ cm) | $Q_{ohm}$ |
|---|---|---|---|
| Aluminum | 3.54 | 3.09 | 32,400 |
| Copper | 5.91 | 2.39 | 41,800 |
| Gold | 4.10 | 2.87 | 34,800 |
| Silver | 6.81 | 2.23 | 44,800 |

[a] *Frequency $f$ = 75 GHz; $\lambda$ = 4 mm; mirror spacing L = 20 mm. Source: American Institute of Physics Handbook, 2nd edition, pp 9-38, McGraw-Hill Book Co., Inc., New York (1963).*

have finite size. The computations have been performed for confocal symmetric resonators [43] and may be extended to any resonator with a symmetry axis. Let the resonator consist of two spherical mirrors, separated by a distance L, of radii of curvature $R_1$ and $R_2$ and diameters $d_1$ and $d_2$, respectively. Then an equivalent confocal resonator can be chosen for each mirror such that the ratio of diameter to beam spot size on the mirror is the same as that of the equivalent confocal system. We define "effective Fresnel numbers" as

$$N_{eff,1} = \frac{d_1^2}{4\pi[w_x(0)]^2} \quad , \tag{44}$$

$$N_{eff,2} = \frac{d_2^2}{4\pi[w_x(L)]^2} \quad , \tag{45}$$

which are the Fresnel numbers of the corresponding equivalent confocal resonators. Once these have been computed, the losses per pass, $\alpha_1$ and $\alpha_2$, can be obtained from Boyd and Gordon [44]. The diffraction Q-factor is then found from

$$Q_{diff} = \frac{4\pi L}{(\alpha_1 + \alpha_2)\lambda} \quad . \tag{46}$$

From Boyd and Gordon, we find that, in order for diffraction losses to be less than the ohmic losses given by equation (43), we must have

$$N_{eff,j} \geq 1.2 \tag{47}$$

for the $TEM_{20}$ mode. For the hemispherical resonator 3, for example, this requires that $d_1 \geq 28$ mm and $d_2 \geq 32$ mm. In practice, the mirror diameters are chosen somewhat larger than these values, and so diffraction losses are small compared with ohmic losses.

Imperfections in the reflector surfaces may also lead to a decrease in the resonator Q. These losses cannot be computed except through a somewhat inexact statistical method; we shall not do so here. They may be minimized by requiring close tolerances in the resonator construction; in this way, it is possible to make these losses small compared to the ohmic losses.

Finally, losses due to output coupling from the resonator, which are discussed in more detail in section 5, must be considered. The normal method of output coupling is by a slit on the surface of resonator 2. The Q-factor corresponding to output coupling is given by equation (39) where P is now the output power. Section 5 demonstrates that coupling is optimum when $Q_{out}$, the output coupling Q, is equal to the unloaded $Q_0$, where

$$\frac{1}{Q_0} = \frac{1}{Q_{ohm}} + \frac{1}{Q_{diff}} + \frac{1}{Q_{scatt}} \quad . \tag{48}$$

In general, the overall cavity Q is

$$\frac{1}{Q_{tot}} = \frac{1}{Q_0} + \frac{1}{Q_{out}} \quad , \tag{49}$$

and so for optimum output coupling we obtain $Q_{tot} = Q_0/2$. For resonators with smooth reflectors, assuming that ohmic losses dominate, we obtain $Q_{tot} \approx 20{,}000$, which is observed experimentally.

### *4.2 Experimental Studies*

The primary problem in extending the 4-mm work of the Soviet orotrons to the short millimeter and submillimeter ranges is finding good resonator designs. By a "good resonator design" we mean one for which the field spot size

on the mirror containing the diffraction grating is of optimum size, the Q is sufficiently high for the modes of interest, and the field amplitude is sufficiently high in the region of the grating to obtain reasonably strong electron-field interaction. The theory outlined above should serve as a useful guide in designing such resonators; however, experimental studies are necessary to complete the designs. Fortunately, these studies have already progressed to a high level of sophistication, and may be grouped into two areas: cold studies of resonators alone, and studies of operating orotrons.

### *4.2.1 Cold Studies*

Cold studies consist of measurements of the Q-factor of resonators and the electromagnetic field distributions within the resonators. Highly sophisticated methods have been devised [44] for making these measurements; we will not discuss these methods here except to say that they involve introducing a small scattering or absorbing probe into the resonator and measuring either the change in the resonator Q or the change in the output power.

In the first operating orotrons, resonators with the plane mirrors completely covered by diffraction gratings were used [45]. It is of interest to compare these resonators with corresponding resonators with smooth mirrors. Consider two hemispherical resonators, with dimensions $R_{sph}$ = 180 mm, $d_{sph}$ = 74 mm, and $d_{p\ell}$ = 70 mm. One of these resonators has a plane mirror covered by a diffraction grating with parameters $\ell$ = 0.9 mm, d = 0.4 mm, and h = 2.75 mm (see sect. 3 for the definition of these grating parameters).

Figure 12 shows the Q-factor of these resonators, for $\lambda$ = 4 mm, as a function of the distance L between the mirrors ($L/R_{sph}$ is the relative distance). Note the dramatic decrease in the resonator Q when one of the mirrors is covered with a grating. In this case, the Q is also sensitive to the particular transverse mode excited in the resonator. Curve 2 is of particular interest; the Q of the $TEM_{20}$ mode for $0.45 \leq L/R_{sph} \leq 0.6$ is about 6000.

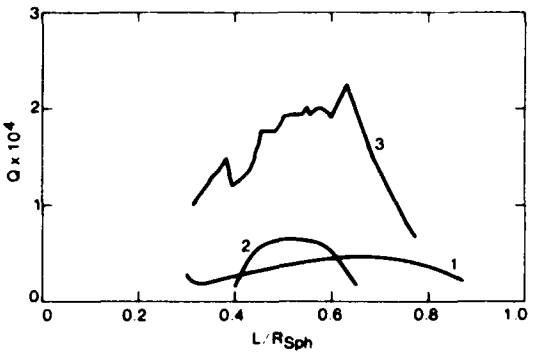


**Figure 12. Dependence of Q-factor on distance between mirrors for hemispherical resonators: (1) resonator with grating, $TEM_{10}$, (2) resonator with grating, $TEM_{20}$, and (3) resonator with smooth mirrors.**

Another quantity of interest is the number of modes for a given separation L whose Q are sufficiently high to allow excitation of these modes. This information is often presented in the form of a histogram with $L/R_{sph}$ plotted on the vertical axis, with each mode (nm) represented as a vertical bar whose extent gives the range of $L/R_{sph}$ over which the mode can be excited. We shall not present this information here, but we summarize it by stating that 11 distinct modes can be excited in both the above resonators [46] for $0.4\ R_{sph} < L < R_{sph}$.

Later orotrons have diffraction strip gratings which cover only a portion of the plane mirror. These resonators have a thinner mode spectrum compared with those considered above. For instance, with a grating width of B = 5 mm (other parameters remaining the same as above), such a resonator could only support three modes for $0.35\ R_{sph} < L < R_{sph}$. This fact makes these resonators particularly appropriate for use in orotrons.

In addition to having a high Q, the resonators used in operating orotrons should have a large electric field near the grating. Studies were performed [47] in which the position of the grating surface relative to the plane mirror surface in a

hemispherical resonator was variable. At a wavelength of $\lambda = 4$ mm, it was found that raising the grating by $z_0 = 0.6$ mm above the plane mirror dramatically enhanced the field distribution near the grating.

Spherocylindrical resonators have been suggested to improve the electron-beam/resonator field coupling in orotrons. Studies performed on spherocylindrical resonators [48] indicate that these resonators with smooth reflectors can support up to 28 modes. However, when a strip grating is applied along the axis of the cylindrical mirror, the mode spectrum is rarefied considerably. The Q-values of the various oscillations in these resonators remained high when the mirror spacing L was lowered to 0.15 $R_{sph}$, as opposed to the hemispherical resonators; in addition, the field amplitudes at the grating were also high when the Q-factor was high, which is seldom the case in hemispherical resonators. These qualities of spherocylindrical resonators make them appropriate for use in compact orotrons. It is found that $TEM_{20}$ modes are most easily excited, although nearly all the excitable modes are suitable for use in orotrons.

Coupling of output power in orotrons of short millimeter and submillimeter range becomes difficult when conventional methods are used (see sect. 5); as a possible solution of this problem, an open toroidal resonator was developed [49]. This resonator allows output coupling through a large hole in the center. Figure 13 shows such a resonator. Studies show that such resonators may indeed be the best ones to use at shorter wavelengths.

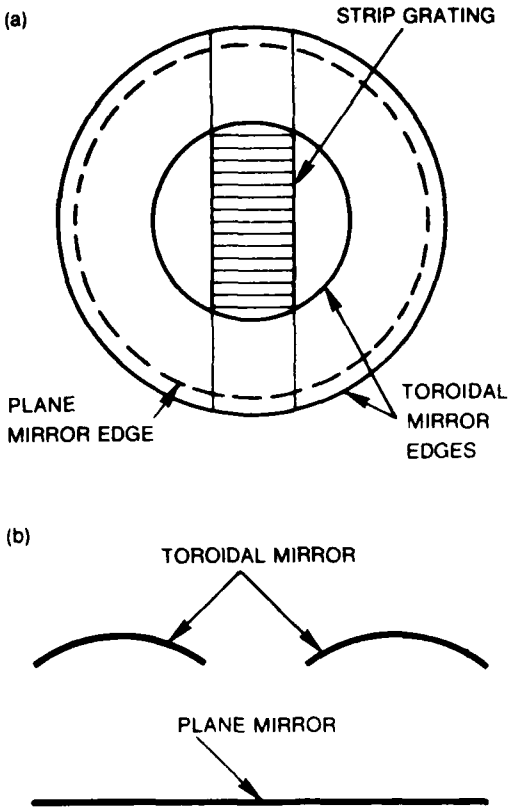


**Figure 13. Toridal resonator: (a) top view and (b) side view.**

### *4.2.2 Operating Orotrons*

It is of interest to compare the performances of various resonator designs in operating orotrons. First, it is interesting that the $TEM_{20}$ mode is the most easily excitable; for example, we compare this mode with the $TEM_{21}$ mode [23].

$TEM_{20}$: $P_{out} = 1.2$ W; $I_{operating} = 140$ mA;

$I_{starting} = 90$ mA

$TEM_{21}$: $P_{out} = 0.03$ W; $I_{operating} = 160$ mA;

$I_{starting} = 140$ mA

Other modes can be excited, but this occurs very rarely and with much higher starting currents.

A study was performed [50] in which orotrons having various spherocylindrical resonators were compared. The radius of the spherical mirror remained constant at $R_{sph} = 110$ mm while the radius of the cylindrical mirror varied. Gratings were used whose parameters (see sect. 3) were $\ell = 0.4$ mm, $d = 0.15$ mm, $h = 0.88$ mm, and width $B = 10$ mm. Energy was withdrawn from a coupling slot $0.1 \times 3.6$ mm$^2$ in the center of the spherical mirror. Results of the investigation are summarized in table 4.

**TABLE 4. SUMMARY OF OPERATING CHARACTERISTICS OF VARIOUS OROTRONS WITH SPHEROCYLINDRICAL RESONATORS**

| Parameter | Resonators | | | | | |
|---|---|---|---|---|---|---|
| | 1 | 2 | 3 | 4 | 5 | 6 |
| $R_{sph}$, mm | 110 | 110 | 110 | 110 | 110 | 110 |
| $R_{cyl}$, mm | 60 | 80 | 110 | 150 | 180 | plane mirror |
| Tuning range, GHz | 69.5 to 79.0 | 67.6 to 78.8 | 67.4 to 78.9 | 67.8 to 79.0 | 69.6 to 79.2 | 71.2 to 78 |
| $I_{starting}$, min, mA | 25 | 21 | 21 | 28 | 51 | 55 |
| $I_{starting}$, mean, mA | 33 | 26 | 28 | 35 | 55 | 60 |
| $P_{mean}$, W | 0.64 | 0.75 | 0.70 | 0.58 | 0.38 | 0.30 |
| $P_{max}$, W | 1.02 | 1.18 | 1.1 | 0.96 | 0.78 | 0.65 |

Table 4 shows that orotrons with spherocylindrical resonators with $R_{cyl}$ = 80 to 110 mm (resonators 2 and 3) represent a considerable improvement over hemispherical orotrons, with starting currents reduced by nearly a factor of 3 and power output improved by a factor of 2. The efficiency of the spherocylindrical orotrons is a factor of 4 greater than that of corresponding hemispherical devices. The reason for this increase is that the use of a cylindrical mirror permits the contraction of the field spot in the direction transverse to the motion of the electron beam, while the extent of the field spot along the direction of electron motion is retained. (We note in passing that the formulas of sect. 4.1 yield spot sizes that are too small by a factor of about 0.67.)

Spherocylindrical orotrons have been made in batch quantities in the Soviet Union which have $R_{cyl} = R_{sph} = 110$; these give output powers up to 1 W at 57 to 70 GHz in a magnetic field of 1.25 kG,* with an operating current of 150 mA. When the magnetic field is increased to 4 kG, the output power reaches 6 W, with a tuning range of an octave. Similar devices were built to operate in the 2-mm range in a magnetic field of 3.8 kG, with output power exceeding 2 W with an operating current of 240 mA at f = 137 GHz.

In order to improve the interaction of the electron beam with the resonator field at smaller wavelengths, it is necessary to stretch the field spot along the reflecting diffraction grating. For this purpose, orotrons were designed [52] which used paired cylindrical mirrors (fig. 14). Results of a study in the 4-mm range [52] indicate that an optimum configuration with $D_{12}$ = 6 mm and $R_{cyl}$ = 80 mm gives an output power of 2.25 W, with an operating current of 130 mA at 57 to 74 GHz. The starting current for this device is 29 mA, making this configuration comparable to the spherocylindrical resonator described earlier.

By using paired spheroidal mirrors in a scheme similar to that shown in figure 14, a Russian team [51] created an orotron operating in the submillimeter range. The curvature radius of the lower mirror was $R_{cyl}$ = 110 mm. A grating 7 mm wide was employed, with $\ell$ = 0.08 mm, d = 0.03 mm, and h = 0.19 mm. The electron-beam cross section was 3.5 × 0.2 mm². The

*(Tesla) = (Gauss) × 10⁻⁴

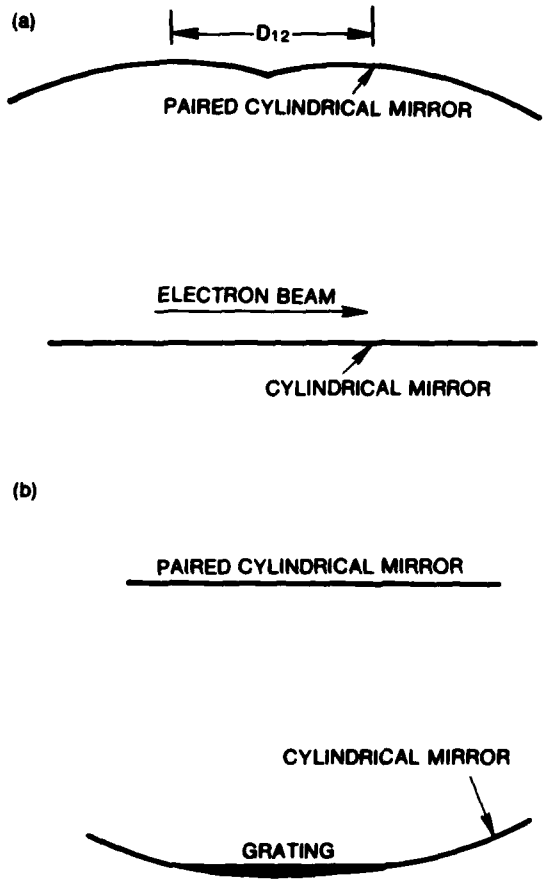


**Figure 14. Resonator with paired cylindrical mirrors: (a) side view and (b) front view.**

curvature radii of the two spheroids forming the upper mirror were 240 mm along the electron trajectory, and 80 mm in a direction perpendicular to the electron trajectory. The separation $D_{12}$ was 10 mm. Power outputs of 60 mW were obtained with starting currents of 140 mA, in the frequency range from 275 to 360 GHz. Operating voltages for these devices were in the 2-kV range.

Toroidal resonators have also been used in operating orotrons [53], for the reasons discussed earlier. Maximum power outputs of 300 mW were obtained at accelerating voltages of 2270 V ($\lambda$ = 4.75 mm) and 2980 V ($\lambda$ = 4.325 mm).

## 5. OUTPUT COUPLING IN OROTRONS

A critical problem in the design of orotrons is that of determining a practical method of extracting power from the open resonator. Various schemes have been devised for this purpose; their utility depends upon the wavelength of operation of the device as well as the design of the open resonator. In this section we examine these schemes.

Consider an open resonator, whose quality factor is Q, into which energy is deposited at a rate P. Let the quality factor of the resonator with no output coupling be $Q_0$, and the correction due to coupling be $Q_{out}$, such that

$$\frac{1}{Q} = \frac{1}{Q_0} + \frac{1}{Q_{out}} \quad . \qquad (50)$$

Let the total energy stored in the resonator be U. In equilibrium we have (see sect. 4)

$$\frac{dU}{dt} = 0 = P - \frac{\omega U}{Q} \quad , \qquad (51)$$

so that $U = \frac{QP}{\omega}$. The output power is given by

$$P_{out} = \frac{\omega U}{Q_{out}} = \frac{Q}{Q_{out}} P \quad . \qquad (52)$$

But according to the theory of bunching (sect. 2), the power radiated by the electron beam in the resonator is proportional to the overall resonator Q. Therefore we have

$$P_{out} \alpha \frac{Q^2}{Q_{out}} = \frac{Q_0^2 Q_{out}}{(Q_0 + Q_{out})^2} \quad . \qquad (53)$$

Output power from the device is at a maximum, when, in equation (53),

$$Q_{out} = Q_0 \quad . \qquad (54)$$

This important relation determines the methods of output coupling appropriate for a particular resonator design and wavelength. Methods of output

coupling fall into two general classes: (1) waveguide coupling and (2) quasi-optic coupling.

The most common method of output coupling [22, 45, 53] in orotrons is waveguide coupling through a slot in the smooth mirror of the device. Figure 15 shows how this coupling is effected. The polarization of the orotron radiation is such that the H-field is out of the paper in the figure. The length of the output coupling slot is approximately equal to the wavelength of radiation; the width is much less than the wavelength. For example, in the experiments discussed in section 4 at $\lambda = 4$ mm, a coupling slot of dimensions $3.6 \times 0.1$ mm$^2$ was used. While this output coupling scheme may be appropriate for this wavelength, the dimensions of the slot are difficult to control as the wavelength is lowered, and the output coupling factor $Q_{out}$ is extremely sensitive to these dimensions.

An alternative to the central coupling slot is an aperture near the periphery of the smooth mirror. For example, orotrons have been designed and built [54] in which the coupling aperture of 4 mm diameter was at the periphery of the smooth mirror in a hemispherical open resonator. By rotating the smooth mirror about the resonator axis, it is possible to vary the degree of coupling in the device. The cross-sectional area of a coupling aperture near the mirror periphery can be much larger than that of a central aperture, and still have the same $Q_{out}$. Thus this method can be used to obtain more precisely controllable output coupling in orotrons operating at wavelengths less than 2 mm. Another alternative* is the use of several small circular holes at the center of the smooth mirror. Figure 16 illustrates this coupling scheme.

All the above coupling schemes rely on waveguides to transmit the energy from the orotron to the load or detector. This is the most convenient way to transmit energy in the millimeter wave range. Waveguides are commercially available which operate in the fundamental mode between 75 and 300 GHz; however, their cost increases dramatically as the frequency increases. Beyond

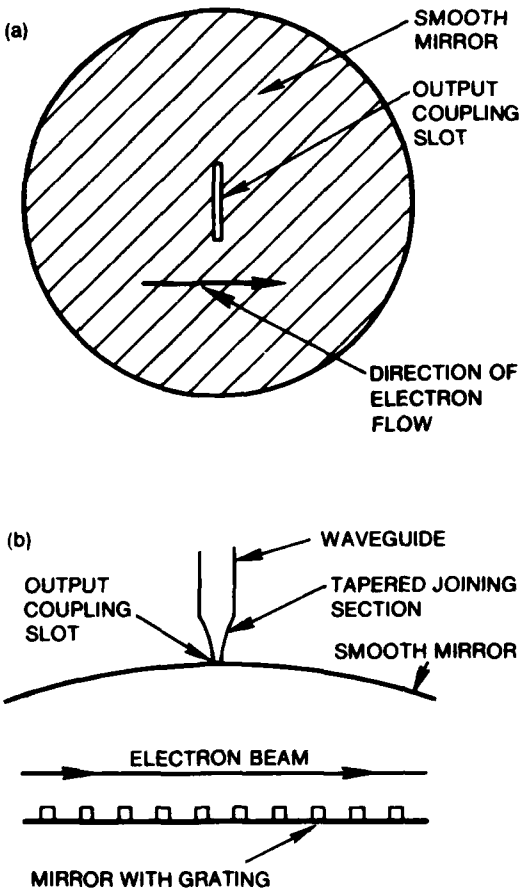


Figure 15. Waveguide coupling: (a) with smooth mirror and (b) orotron (side view) with output coupling.

350 GHz, other schemes must be devised wherein the radiation emitted by the orotron propagates through free space. We discuss three of these schemes.

The toroidal resonator, discussed in section 4, has its energy output coupled into free space through the large hole in its center. Essentially, the diffraction losses in such a device represent the power output. Radiation escaping through this hole forms a collimated beam which propagates in a direction along the axis of symmetry of the resonator. The output coupling factor $Q_{out}$ can be controlled rather precisely by judicious design of the

* *We are indebted to Herb Dropkin of HDL for this suggestion.*

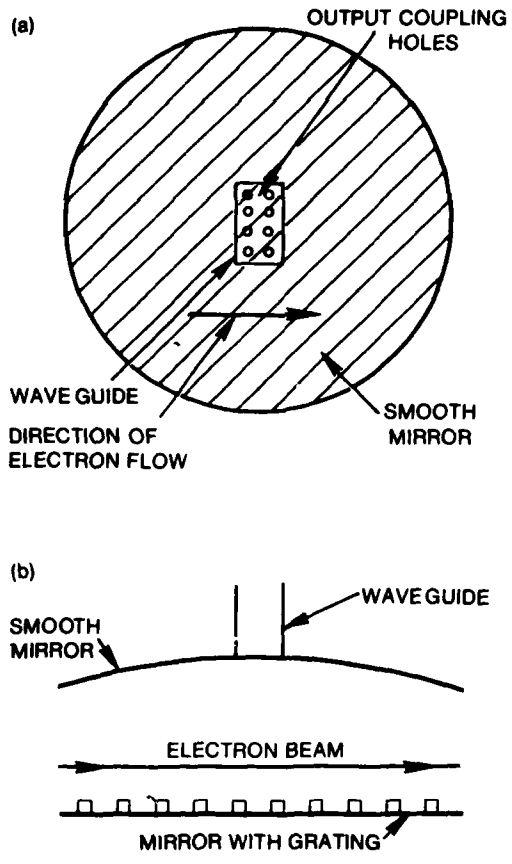


Figure 16. Waveguide-holes coupling: (a) smooth mirror and (b) orotron (side view) with output coupling.

resonator, but, once fixed, cannot be varied. This design, however, is very appropriate for small wavelengths (~1 mm).

Another extremely important output coupling design replaces the smooth mirror of the resonator by a semitransparent surface. For example, a strip grating may be deposited on a converging lens [55, 56], as shown in figure 17. Power outputs up to 2 W have been obtained in orotrons built with this type of output coupling. The degree of coupling may be continuously varied by rotating the lens-grating system about the resonator axis. At a rotation angle of 5 degrees from the position shown in figure 17, the output power is a maximum.

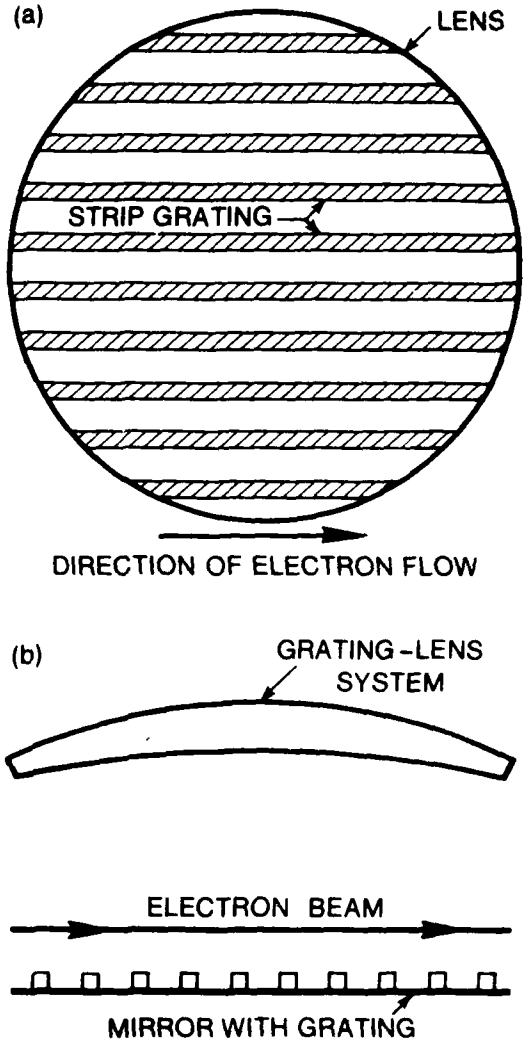


Figure 17. Quasi-optical coupling: (a) partially transmitting mirror and (b) orotron (side view).

It has been suggested* that an unstable resonator design might make better use of the active volume of an orotron and lead to improved output coupling. However, the success of unstable resonators in lasers, for example, depends on a high gain medium. In laser terms, the "gain" of the orotron is relatively low; therefore the unstable resonator idea cannot be used in the same manner

* *Colin Willett of HDL suggested the use of unstable resonators in orotrons*

as in lasers. However, it is possible to design a resonator system in which the diffraction losses may be used as output power, and which has a stable, high-Q cavity. The advantage of this system is that the output coupling does not represent an additional loss; for a fixed-size resonator, the diffraction losses are unavoidable, and so use of those losses represents the most efficient use of the resonator system. Because of these facts, it was possible [57] to design an orotron operating in the 4-mm range in which the starting currents ranged from 7 to 13 mA, the lowest starting currents we have been able to find in the Soviet literature.

In summary, several output coupling schemes have appeared in the literature, and have been suggested to the present authors. Each of these schemes needs to be considered in detail with regard to

(1) its effect on the operating parameters of the orotron,
(2) its appropriateness at wavelengths from 1 to 2 mm, and
(3) simplicity of construction.

## 6. ELECTRON GUNS USED IN OROTRONS

Although a well-controlled, ribbon-shaped electron beam (e-beam) is required for the operation of the orotron, very little information has been published in the literature on the design of the electron guns used in these devices. The Japanese reported only [27] that a convergent electron gun produced a ribbon-like e-beam 20 × 0.3 mm², and a magnetic field of 4 kG was necessary for proper beam focusing. Their gun was operated under pulsed conditions (2 μs, 50 Hz) at a beam voltage of 6 to 20 kV and beam density of 20 to 30 A/cm². The Russians seem to have used [23, 45, 58] nonconvergent diode guns. Rather than describe their guns, they too described only the beams in terms of starting currents and voltages for beams of given dimensions. Rusin and Bogomolov, for example, reported that they first [45] used a diode gun to produce a 3.5 × 0.5 mm² ribbon-like beam which was cut out by means of a diaphragm. This beam was accelerated by various voltages between 1.5 and 9.0 kV. In addition they observed that radiation was generated at starting currents of 100 mA; they also reported that they kept the beam rigid by placing the entire system between flat pole pieces of an electromagnet, which produced a uniform field directed along the beam with induction up to 5.5 kG. Similar results were reported [23, 58] elsewhere; the thinnest reported [58] beam was 0.2 × 5 mm, and it was kept rigid by a 3.8-kG magnetic field directed along the beam. In building an orotron, we are guided by this type of information. To design the gun, however, we shall follow the methods of Pierce [59] to obtain space-charge-flow solutions for our system, which requires a thin sheet (ribbon) beam.

### *6.1 Theoretical Considerations*

In this work we consider rectilinear flow in a planar diode since this seems to be appropriate for the type of gun that the Russians used. As we gain more experience in orotron design, we will consider other types of guns such as temperature-limited guns, which use cold cathodes, and convergence guns. The electron flow is confined in the case that we will consider, and we will assume that the gun operates under space-charge-limited conditions. Space-charge-limited flow is defined [60] as a flow in which the current drawn from the cathode is independent of the maximum emission current from the cathode. It depends only on the potentials applied to the electrodes of the system and, hence, on the space charge itself. In addition, we give here the theoretical results presented by Pierce [59]. In that work it is assumed that the electron flow is along parallel paths in the y-direction with a uniform current density J. Then, neglecting magnetic effects, we have

$$\frac{d^2V}{dy^2} = \frac{J}{\varepsilon_0 \sqrt{2\eta V}} \quad . \tag{55}$$

where V is the potential, $\eta = e/m$ ($\eta = 1.759 \times 10^{11}$ C/kg, e is the electronic charge, and m is electron mass), and $\varepsilon_0$ is the permittivity of free

space ($\varepsilon_0 = 8.854 \times 10^{-12}$ F/m). Taking V = 0 at the origin, the solution of equation (55) is

$$V = A\, y^{4/3} \quad , \tag{56}$$

where

$$A = \left[\frac{9\,J}{4\varepsilon_0(2\eta)^{1/2}}\right]^{2/3} = 5.69 \times 10^3\, J^{2/3} \quad . \tag{57}$$

This solution of equation (55) describes electron flow in the region between infinite parallel-plane equipotential surfaces. Also, such flow exists in a region bounded by planes parallel to the flow with the space outside this region being free of charge. In this case, the fields outside the flow are determined by conditions at the boundary between the charge-free region and the region occupied by the flow.

In order to describe a beam of finite thickness, the potential must satisfy Laplace's equation in the charge-free region subject to the boundary conditions

$$\frac{\partial V}{\partial x} = \frac{\partial V}{\partial z} = 0 \tag{58}$$

and V = f(y) at z = 0, where the edge of the beam is at z = 0. A solution of Laplace's equation for which V = f(y) at z = 0 is

$$V = \text{Real } A\,(y + iz)^{4/3} \quad . \tag{59}$$

Letting $y = r\cos\theta$ and $z = r\sin\theta$, this says that V is proportional to $r^{4/3}\cos 4\theta/3$. The shape of the equipotentials is independent of the absolute magnitude of the potentials involved and of the units in which distance is measured. With the cathode taken at zero potential, Pierce [59] shows that the zero potential surface in the charge-free region is a plane which meets the edge of the cathode at y = z = 0, making an angle of 67.5 deg with the normal to the cathode (the y-axis); this is from equation (59).

Figure 18 shows how these results may be incorporated to produce a parallel flowing beam. If a sufficiently strong magnetic field is applied along the beam (from 1 to 5 kG) to keep the beam rigid, this parallel flowing beam may be guided over the orotron grating.

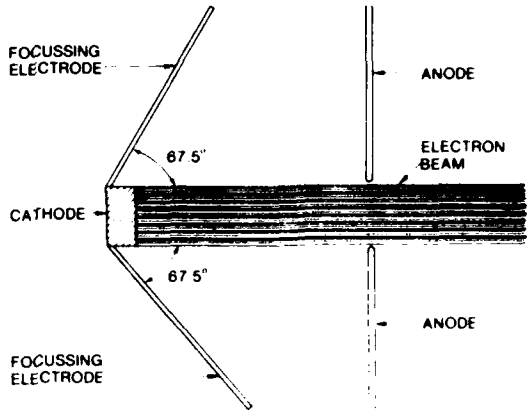


**Figure 18. Pierce gun design.**

### *6.2 Electron Gun Design*

It has been suggested* that the simple theory presented in section 6.1 is sufficient to describe qualitatively the electron flow in orotron systems such as those described by the Russians [23, 45, 58]. In an attempt to go beyond the simplest system, however, we have obtained from W. Herrmannsfeldt of the Stanford Linear Accelerator Center (SLAC) a rather sophisticated electron trajectory computer program [61] for use on the HDL IBM 370/168 system. In this program, we can put in the positions of the cathode, anode, and focussing electrodes, and specify boundary conditions imposed by the various applied voltages and magnetic fields. The program then calculates electron trajectories by using fields determined by differentiating the potential distribution. The electron trajectory equations are fully relativistic and account for all possible electric and magnetic field components.

The electron-trajectory program may be used in either rectangular or cylindrical coordinates. In cylindrical coordinates the magnetic fields are axially symmetric, and it is this mode of operation which is of most interest here. The origin can

* *Karp, A., and Miram, G. of Varian Associates in Palo Alto, CA (private communication).*

be offset so that the geometry approaches the rectangular coordinate situation. The SLAC program, when used in rectangular coordinates, considers the external magnetic field to be normal to the beam.

After the input data are read in with the appropriate geometry and boundary conditions, the program first solves Laplace's equation. Next the electron trajectories are started where the assumption is made that Child's law [62] holds near the cathode. On the first iteration of the program, space charged forces are calculated from the assumption of paraxial flow [59]. After all the electron trajectories have been calculated, the program begins the second cycle by solving Poisson's equation with the space charge from the first iteration.

The Child's law calculations for the starting conditions are remade for every iteration. The perveance (defined as equal to $V/I^{3/2}$ where V is the beam accelerating voltage and I the beam current) converges in an iterative process in which the program averages the perveance used for the previous iteration with the perveance calculated directly from the solution of Poisson's equation.

Self-magnetic fields are calculated from the current in the rays on the present cycle. This calculation assumes that all the current from the previous rays lies on the axis of an infinitely long conductor. If the ray being calculated crosses the last preceding ray, then the current from that ray is dropped, provided that the first ray does not continue to cross the rays. Also, the ray is terminated if it dips more than one grid point below the surface of an electrode.

Figures 19 and 20 are representative outputs which can be obtained from the electron trajectory program. Figure 19 gives the electron trajectories and equipotential surfaces calculated for the system in rectangular coordinates. Since no magnetic field is applied, the beam tends to pull apart, and many of the rays terminate on the lower metal surface which is at the anode potential. Figure 20 shows the effect of applying a uniform magnetic field of 2000 G in the direction along the beam. The beam no longer pulls apart but would not be suitable for orotron operation since it does not flow uniformly. If the potential is changed to −250 V on the focussing electrode, a uniform beam that does not pinch together at the anode is generated. Other changes, such as varying the

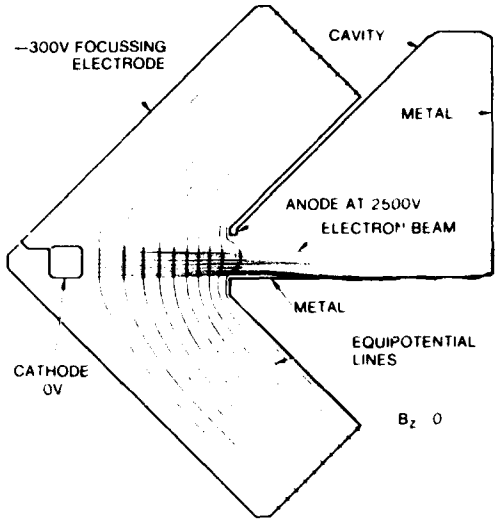


**Figure 19. Sample problem for electron trajectory code (no magnetic field).**

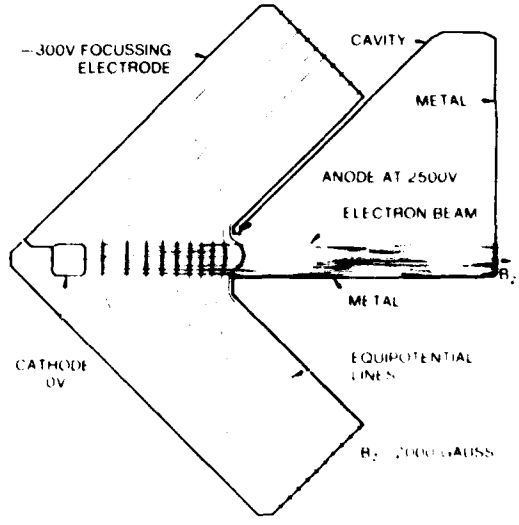


**Figure 20. Same problem as Figure 19, with $B_z$ = 2000 G.**

position of the cathode or changing the angle of the focussing electrodes, can be made. In this manner one can determine a suitable design for an electron gun and can plot the behavior of the beam as various voltages or magnetic fields are applied to the system.

## 7. CONCLUDING REMARKS

The fundamental mechanism of the orotron is well understood; that is, Smith-Purcell radiation by an electron beam passing over a grating combined with feedback due to the open resonator gives rise to coherent radiation at a specified wavelength. The basic theory of Smith-Purcell radiation, as outlined in section 2, gave the relation between beam accelerating voltage, grating period, and emission wavelength. The theory of electron bunching predicts the condition (i.e., starting beam current) under which coherent emission can be obtained.

In addition to predicting the wavelength of emission, a theory of the Smith-Purcell effect should also be able to predict optimum values of the grating groove depth and width. These predictions were discussed in more detail in sections 3 and 4, and recommendations made concerning Smith-Purcell theory, in section 3.

The theory of electron bunching is presently at a very crude stage. The following improvements should be made in the theory.

(1) Modification of the resonator mode field by the diffraction grating should be taken into account as was discussed in section 3.

(2) All the energy radiated by the electron beam is *not* used by the resonator, a large fraction being lost into free space (i.e., out the sides of the resonator).

(3) Repulsion of electrons by other electrons in the beam has not been accounted for. This repulsion places an upper limit on the current density of the beam.

(4) Nonlinearities in the rf field must be taken into account. This is necessary in order to predict output powers and efficiencies of orotrons. The present linear theory can only predict the starting current.

(5) An estimate must be made of the spectral purity of the radiation emanating from the orotron. So far, we have been unable to find anywhere in the literature a theoretical estimate or an experimental measurement of this important quantity.

The influence of the grating on the resonator modes should be calculable in an approximate manner based on the formalism described in section 3. Of primary interest is the amplitude of the field distribution near the grating, which determines the strength of the beam-resonator coupling. It is also desirable that a computer program be written exploiting the formulas derived by the Soviets for Smith-Purcell radiation from comb gratings. In this manner, we can verify the performance characteristics of the gratings and use this approach to design gratings required for orotrons that operate in the 1 to 2 mm wavelength region.

The theoretical formalism developed in section 4.1 is not entirely appropriate for designing orotron resonators for use in the range $4\text{ mm} > \lambda > 1\text{ mm}$. The reason for this is that the condition $w >> \lambda$, on which the theory is based, is not satisfied. Experimental evidence for this is discussed in section 4.2, where experimental resonator spot sizes were found to be larger than those calculated in section 4.1 by about 1.5. If theoretical predictions are to serve as a guide in designing resonators, then this deficiency must be remedied. In particular, the width of the resonator beam in the direction transverse to the electron beam motion is a critical parameter; it must be chosen so that the minimum (at $x/w = \frac{1}{2}$) of the $TEM_{20}$ mode falls exactly on the edge of the strip grating.

Beam modes in arbitrary resonators may be computed numerically to any desired degree of accuracy by the solution of an integral equation. These computations would avoid the approximations inherent in the formalism of section 4.1, and

also would allow computation of diffraction losses for resonators of any desired shape. Thus, some of the more complex resonator designs discussed in section 4.2 would lend themselves to analysis. Any reasonable orotron development program should include the facility for performing these computations. For this reason, we give high priority to the task of performing numerical mode computations for arbitrary resonators.

An experimental facility should have radiation sources available (e.g., klystrons) in the wavelength ranges in which proposed orotrons are to be built. Cold testing of resonators should include measurement of Q-values and crude measurements of field distribution within the resonator. The level of sophistication need not be near that of the Soviets, as most of the desired information is already known.

A variety of resonator designs should be considered in constructing orotrons for the NMMW range. In section 4 some possibilities were outlined; however, the number of potential candidates is limitless. Choice of efficient configurations for a particular application is an art as well as a science; the task is facilitated, however, by proper theoretical guidance. Nevertheless, one should not be prevented from using a trial-and-error approach in testing out new ideas since the cost of resonator mirrors is not severe.

In section 5, several output coupling schemes for orotrons were discussed; further work is needed in this area. In addition, in section 6 it was pointed out that in order to build an orotron, a thin strip beam has to be formed, launched, accelerated, focussed, and collected. Since all this has to be integrated with the slow wave structure (i.e., the grating and cavity), the task seems somewhat difficult. A few attempts have been made in the U.S. to use strip beams in traveling wave tubes and backward wave oscillators. However, because the e-beams used in these devices were unstable, these projects were abandoned. Since the Russians have been successful in building efficient orotrons which use strip beams, we explored the problems with W. Herrmannsfeldt of SLAC and personnel of Varian Associates, Northrop, Litton, and Raytheon. It was concluded that we should be able to repeat the Russian work since the beam requirements are not as stringent as for certain other devices, such as the traveling wave tube worked on earlier by Varian.

The behavior requirements for the gun will be worked out at HDL. The SLAC program, run on the HDL computer, can be used to determine the sensitivity of the beam to positions of the electrodes, to voltages applied to the necessary electrodes, and to the shape and strength of the applied magnetic field. Outside contractors have offered to provide technical information and assistance to assure that the proper materials are selected. For example, magnetic material cannot be used in the gun since it is to be immersed in the magnetic field. Materials that have the correct thermal properties will have to be chosen so that the mechanical positions of the electrodes remain intact as the gun heats up. Proper insulation and appropriate connectors must be selected, and many of these details are well known to skilled e-beam gun manufacturers. Industrial contractors, such as those mentioned above, can provide their expertise in determining suitable cathodes for the gun which can produce required current densities (5 $A/cm^2$) and yet have relatively long operating lifetimes (up to 5000 hours).

## LITERATURE CITED


1. J. C. Slater, Microwave Electronics, D. Van Nostrand Company, Inc., New York (1950).
2. J. M. Manley and H. E. Rowe, Proc. IRE *47* (1959), 2115.
3. M. Danos, J. Appl. Phys. *26* (1955), 2.
4. H. Lashinsky, J. Appl. Phys. *27* (1956), 631.
5. H. Mendlowitz and S. J. Glass, Phys. Rev. D *15* (1977), 530.
6. J. E. Walsh, T. C. Marshall, M. R. Mross, and S. P. Schlesinger, IEEE Trans. Microwave Theory and Techniques (1977).
7. C. K. Chen, J. C. Sheppard, M. A. Piestreys, and R. H. Pantell, J. Appl. Phys. *49* (1978), 41.
8. M. Danos, S. Geschwind, H. Lashinsky, and A.Van Trier, Phys. Rev. (1954).
9. P. D. Coleman and C. Enderby, J. Appl. Phys. *31* (1960), 1695.
10. J. E. Walsh, T. C. Marshall, and S. P. Schlesinger, Bull. APS *21* (1976), 692.
11. F. A. Hopf, P. Meystre, and M. O. Scully, Phys. Rev. Lett. *37* (1976), 1215.
12. D. A. G. Deacon, L. R. Flias, J. M. J. Madey, G. J. Ramian, H. A. Schwettman, and T. I. Smith, Phys. Rev. Lett. *38* (1977), 892.
13. T. Kwan, J. M. Dawson, and A. T. Lin, Phys. Fluids *20* (1977), 581.
14. I. B. Bernstein and J. L. Hirshfield, Phys. Rev. Lett. *40* (1978), 761.
15. S. Schneider and R. Spitzer, Nature *250* (1974), 643.
16. A. V. Gaponov, A. L. Goldenberg, D. P. Grigorev, I. M. Orlova, T. B. Pankratova, and M. I. Petelin, JETP *2* (1965), 430.
17. A. V. Gaponov, M. I. Petelin, and V. K. Yulpatov, Radiophys. *10* (1967), 1414.
18. S. J. Smith and E. M. Purcell, Phys. Rev. *92* (1953), 1069.
19. I. M. Frank, IZV AN SSSR, Physics Series, *6* (1942), 3.
20. F. S. Rusin and G. D. Bogomolov, Soviet Patent No. 195557 (1965).
21. N. Tagushi and S. Ono, Report of Research Group on Electron Devices (March 1964) (in Japanese).
22. K. Mizuno, S. Ono, and Y. Shibata, IEEE Trans. Electron Devices *20* (1973), 749.
23. V. P. Shestopalov, Diffraction Electronics, Khar'kov (1976) (Translation by U.S. Joint Publications Service, April 1978).
24. C. W. Barnes and K. G. Dedrick, J. Appl. Phys. *37* (1966), 411.
25. I. Palocz and A. A. Oliner, Proc. IEEE 55 (1967), 46.
26. P. M. van der Berg and T. H. Tan, JOSA *64* (1974), 325.
27. G. Toraldo di Francia, Nuovo Cimento, Ser. X, *16* (1960), 61.
28. B. M. Bolotovskii and A. K. Burtsen, Optics and Spectroscopy *19* (1965), 263.
29. S. J. Glass and H. Mendlowitz, Phys. Rev. *174* (1968), 57.

## LITERATURE CITED (cont'd)


30. W. W. Salisbury, Electronics Magazine (October 19, 1962) p 74.

31. J. P. Bachheimer, Phys. Rev. B *6* (1972), 2985.

32. B. M. Bolotovskii and G. V. Voskresenskii, Usp. Fiz. Nauk. *94* (1968), 377.

33. I. Palocz, Proc IEEE 55 (1967), 46.

34. A. Gover and A. Yariv, J. Appl. Phys. *16* (1978), 121.

35. R. D. Hazeltine, M. N. Rosenbluth, and A. M. Sessler, J. Math. Phys. *12* (1971), 502.

36. J. Lam, J. Math. Phys. *8* (1967), 1053.

37. O. A. Tret'yakov, S. S. Tret'yakov, and V. P. Shestopalov, Radio Eng. Elect. Phys. *10* (1964), 1059.

38. A. Yariv, Quantum Electronics, 2nd edition, John Wiley & Sons, Inc., New York (1975), pp 109-110.

39. L. Casperson, Modes and spectra of high gain lasers, Ph.D. Thesis, California Institute of Technology (1971).

40. E. D. Rainville, Special Functions,The Macmillan Company, New York (1960), p 130.

41. J. D. Jackson, Classical Electrodynamics, John Wiley & Sons, Inc., New York (1963), pp 236-240.

42. A. G. Fox and T. Li, Bell System Tech. J. *40* (1961), 453.

43. G. D. Boyd and J. P. Gordon, Bell System Tech. J. *40* (1961), 489.

44. A. A. Petrushin, I. M. Balaklitskiy, and V. P. Shestopalov, A Device for the Visualization of Electromagnetic Fields in Open Resonators, Soviet Patent No. 286004 (1969).

45. F. S. Rusin and G. D. Bogomolov, JETP letters *4* (1966), 160.

46. I. M. Balaklitskiy and A. A. Petrushin, Investigation of Open Resonators Used in Diffraction Electronics, in Radioteckhnika (Radio Engineering), No. 7, Kharkov (1968), pp 111-123.

47. A. A. Vertiy, N. A. Popenko, B. K. Skrynnik, et al, Radiophysica *18* (1975), 109.

48. A. P. Koretskiy, V. K. Korniyenkov, A. A. Petrushin, et al, Radiophysica *19* (1976), 1581.

49. A. V. Kamyshan, V. V. Kamyshan, and V. P. Shestopalov, Open Resonator, Soviet Patent No. 362381 (1971).

50. V. K. Korneyenkov, A. A. Petrushin, B. K. Skrynnik, et al, Radiophysica *19* (1976), 812.

51. V. G. Kurin, I. D. Revin, B. K. Skrynnik, et al, Dokl. Ukr. SSR Acad. Sci. *8* (1976), 815.

52. A. V. Kamyshan, A. I. Tsvyk, and V. P. Shestopalov, Radiophysica *17* (1974), 727.

53. V. P. Shestopalov, I. M. Balaklitskiy, O. A. Tret'yakov, et al, Elect. Tech. *12* (1972), 50.

54. V. G. Kurin, B. V. Skrynnik, and V. P. Shestopalov, Radiophysics *19* (1976), 128.

55. G. D. Bogomolov, F. S. Rusin, and V. S. Kushch, Radiotech. & Elect. *15* (1970), 854.

56. I. M. Balaklitskiy, I. D. Revin, V. K. Skrynnik, et al, Radiophysics *16* (1973), 235.

57. A. A. Vertik, V. N. Derkach, N. A. Popenko, et al, Dokl. Ukr. SSR Acad. Sci. *4* (1976), 354.

58. F. S. Rusin and G. D. Bogomolov, Proceedings of the IEEE *57* (1969), 720.

## LITERATURE CITED (cont'd)


59. J. R. Pierce, Theory and Design of Electron Beams, D. Van Nostrand Company, Inc., New York (1954).

60. P. T. Kirstein, G. S. Kino, and W. E. Waters, Space-Charge Flow, McGraw-Hill Book Co., New York (1967), p 48.

61. W. B. Herrmannsfeldt, Electron Trajectory Program, Stanford Linear Accelerator Center, SLAC Report No. 166, Stanford, CA (September 1973).

62. K. R. Spangenberg, Fundamentals of Electronic Devices, McGraw-Hill Book Co., New York (1957).

# DISTRIBUTION

ADMINISTRATOR
DEFENSE DOCUMENTATION CENTER
ATTN DCC-TCA (12 COPIES)
CAMERON STATION
ALEXANDRIA, VA 22314

COMMANDER
US ARMY RSCH & STD GP (EUR)
ATTN LTC JAMES M. KENNEDY, JR
CHIEF, PHYSICS & MATH BRANCH
FPO NEW YORK 09510

COMMANDER
US ARMY MATERIEL DEVELOPMENT &
READINESS COMMAND
ATTN DRXAM-TL, HQ TECH LIBRARY
ATTN DRCDE, DIR FOR DEVEL & ENGR
ATTN DRCDMD-ST
ATTN DRCBSI, P. DICKERSON
5001 EISENHOWER AVENUE
ALEXANDRIA, VA 22333

COMMANDER
US ARMY ARMAMENT MATERIEL
READINESS COMMAND
ATTN DRSAR-LEP-L, TECHNICAL LIBRARY
ROCK ISLAND, IL 61299

COMMANDER
US ARMY MISSIEL & MUNITIONS
CENTER & SCHOOL
ATTN ATSK-CTD-F
REDSTONE ARSENAL, AL 35809

DIRECTOR
US ARMY MATERIEL SYSTEMS ANALYSIS
ACTIVITY
ATTN DRXSY-MP
ABERDEEN PROVING GROUND, MD 21005

DIRECTOR
US ARMY BALLISTIC LABORATORY
ATTN DRDAR-TSB-S (STINFO)
ATTN DRXBR, DIRECTOR
ATTN DRXBR-TB, F. J. ALLEN
ATTN DRDAR-BLB, R. MCGEE
ATTN DRDAR-BL, H. REED
ABERDEEN PROVING GROUND, MD 21005

TELEDYNE BROWN ENGINEERING
ATTN MS-44, MELVIN L. PRICE
CUMMINGS RESEARCH PARK
HUNTSVILLE, AL 35807

US ARMY ELECTRONICS TECHNOLOGY
AND DEVICES LABORATORY
ATTN DELET-DD
ATTN DELET-B, I. REINGOLD
ATTN DELET-I, H. JACOBS
ATTN DELET-I, A. KERECMAN
FORT MONMOUTH, NJ 07703

COMMANDER
US AIR FORCE GEOPHYSICAL LAB
ATTN S. A. CLOUGH
L. G. HANSCOMB FIELD
BEDFORD, MA 01731

COMMANDER
US AIR FORCE ROME AIR
DEVELOPMENT CENTER
ATTN RADC/ETEN, E. ALTSHULER
L. G. HANSCOMB FIELD
BEDFORD, MA 01730

COMMANDER
US ARMY ATMOSPHERIC
SCIENCES LABORATORY
ATTN H. RACHELLE
ATTN DRSEL-BL-AS-P, K. WHITE
ATTN DRSEL-BL, LIBRARY
WHITE SANDS MISSILE RANGE, NM 88002

COMMANDER
US ARMY FOREIGN SCIENCE AND
TECHNOLOGY CENTER
220 SEVENTH STREET, NE
ATTN DRXST-SD, O. R. HARRIS
CHARLOTTESVILLE, VA 22901

COMMANDER
US ARMY MISSILE COMMAND
ATTN DRSMI-REO, G. EMMONS
ATTN DRDMI-TRO, W. L. GAMBLE
ATTN DRDMI-TRO, B. D. GUENTHER
ATTN DRDMI-TR, R. L. HARTMAN
ATTN DRDMI-TB, REDSTONE SCIENCE
INFORMATION CENTER
ATTN A. H. GREEN
REDSTONE ARSENAL, AL 35809

COMMANDER
US ARMY NIGHT VISION & ELECTRO-OPTICS
LABORATORY
ATTN W. EAIY
ATTN DELNV-VI, J. R. MOULTON
ATTN DELNV-II, R. SHURTZ
ATTN LIBRARY
ATTN DR. R. C. BUSER
ATTN DELNV-L, R. RHODE
ATTN DELNV-R, R. PEARCE
FT BELVOIR, VA 22060

DISTRIBUTION (Cont'd)

COMMANDER
US ARMY RESEARCH OFFICE
ATTN DRXDO-PH, R. LONTZ
ATTN DRXDO-PH, C. BOGHOSIAN
ATTN J. SUTTLE
RESEARCH TRIANGLE PARK
DURHAM, NC 27709

COMMANDER
NAVAL RESEARCH LABORATORY
ATTN V. L. GRANATSTEIN
ATTN CODE 7111, J. P. HOLLINGER
ATTN CODE 7122.1, K. SHIVANANDAN
ATTN CODE 7110, B. YAPLEE
ATTN L. YOUNG
WASHINGTON, DC 20375

COMMANDER
NAVAL SURFACE WEAPONS CENTER
ATTN F-34, J. J. TETI, JR.
DAHLGREN, VA 22448

COMMANDER
NAVAL SURFACE WEAPONS CENTER
ATTN R-42, N. GRIFF
ATTN R-43, A. KRALL
ATTN F-46, R. E. JENSEN
WHITE OAK, MD 20910

COMMANDER
BALLISTIC MISSILE DEFENSE AGENCY
ADVANCED TECHNOLOGY CENTER
ATTN BMD-ATC-D, C. JOHNSON
P.O. BOX 1500
HUNTSVILLE, AL 35807

DEFENSE ADVANCED RESEARCH PROJECTS AGENCY
ATTN TTO, J. TEGNELIA
ATTN STO, S. ZAKANYCZ
1400 WILSON BLVD
ARLINGTON, VA 22209

NASA/GODDARD SPACE FLIGHT CENTER
ATTN CODE 723, N. MCAVOY
GREENBELT, MD 20771

NATIONAL BUREAU OF STANDARDS
ATTN K. M. EVENSON
ATTN R. PHELAN
BOULDER, CO 80302

NATIONAL OCEANOGRAPHIC AND
ATMOSPHERIC ADMINISTRATION
ATTN V. E. DERR
ATTN LIBRARY, R-51 TECH REPORTS
BOULDER, CO 80303

EMORY UNIVERSITY--PHYSICS DEPARTMENT
ATTN S. PERKOWITZ
ATLANTA, GA 30322

ENVIRONMENTAL RESEARCH
INSTITUTE OF MICHIGAN
ATTN M. BAIR
ATTN G. H. SUITS
P.O. BOX 618
ANN ARBOR, MI 48107

FORD-AERONUTRONIC
ATTN D. E. BURCH
FORD ROAD
NEWPORT, CA 92663

GEORGIA INSTITUTE OF TECHNOLOGY
ENGINEERING EXPERIMENT STATION
ATTN J. J. GALLAGHER
ATTN J. WILTSE
ATLANTA, GA 30332

HONEYWELL CORPORATE RESEARCH CENTER
ATTN P. W. KRUSE
10701 LYNDALE AVE, SOUTH
BLOOMINGTON, MN 55420

INSTITUTE FOR DEFENSE ANLAYSES
ATTN V. J. CORCORAN
400 ARMY-NAVY DRIVE
ARLINGTON, VA 22202

THE IVAN A. GETTING LAB
THE AEROSPACE CORPORATION
ATTN E. J. DANIELEWICZ, JR.
ATTN T. S. HARTWICK
ATTN D. T. HODGES
P.O. BOX 92957
LOS ANGELES, CA 90009

LITTON INDUSTRIES, INC.
ELECTRON TUBE DIVISION
ATTN P. BAHR
ATTN J. HULL
ATTN J. MUNGER
1035 WESTMINISTER DRIVE
WILLIAMSPORT, PA 17701

MASS INSTITUTE OF TECHNOLOGY
FRANCIS BITTER NATIONAL
MAGNET LABORATORY
ATTN K. J. BUTTON
ATTN R. J. TEMKIN
170 ALBANY STREET
CAMBRIDGE, MA 02139

MASS INSTITUTE OF TECHNOLOGY
LINCOLN LABORATORY
ATTN C. BLAKE
ATTN H. R. FETTERMAN
ATTN D. TEMME
P.O. BOX 73
LEXINGTON, MA 02173

DISTRIBUTION (Cont'd)

NORTHRUP CORPORTION
DEFENSE SYSTEMS DIVISION
ELECTRON TUBE SECTION
ATTN G. DOEHLER
ATTN O. DOEHLER
ATTN R. ESPINOSA
ATTN R. MOATES
DES PLAINES, IL 60018

R&D ASSOCIATES
ATTN DR. G. GORDON
P.O. BOX 9695
MARINA DEL REY, CA 90291

RAYTHEON COMPANY
MICROWAVE AND POWER TUBE
DIVISION
ATTN L. CLAMPITT
ATTN R. HARPER
FOUNDRY AVENUE
WALTHAM, MA 02154

STANFORD RESEARCH INSTITUTE
ATTN J. WATJEN
3980 EL CAMINO ROAD
PALO ALTO, CA 94306

UNIVERSITY OF ILLINOIS
DEPARTMENT OF ELECTRICAL
ENGINEERING--EERL-200
ATTN P. D. COLEMAN
ATTN T. A. DETEMPLE
URBANA, IL 61801

UNIVERSITY OF LOWELL--NORTH CAMPUS
DEPARTMENT OF PHYSICS AND APPLIED PHYSICS
ATTN D. KORFF
ATTN G. WALDMAN
UNIVERSITY AVENUE
LOWELL, MA 01854

VARIAN ASSOCIATES
PALO ALTO MICROWAVE TUBE DIVISION
ATTN H. JORY
ATTN A. KARP
ATTN E. LIEN
611 HANSEN WAY
PALO ALTO, CA 94303

US ARMY ELECTRONICS RESEARCH
& DEVELOPMENT COMMAND
ATTN TECHNICAL DIRECTOR, DRDEL-CT
ATTN J. SCALES, DRDEL-AP-CCM
ATTN D. GIGLIO, DRDEL-AP-CCM
ATTN B. ZARWYN, DRDEL-AP-OA

HARRY DIAMOND LABORATORIES
ATTN CO/TD/TSO/DIVISION DIRECTORS
ATTN RECORD COPY, 81200
ATTN HDL LIBRARY, 81100 (3 COPIES)
ATTN HDL LIBRARY, 81100 (WOODBRIDGE)
ATTN CHAIRMAN, EDITORIAL COMMITTEE
ATTN TECHNICAL REPORTS BRANCH, 81300
ATTN CHAIRMAN, EDITORIAL COMMITTEE
ATTN H. DROPKIN, 11100
ATTN H. GERLACH, 11100
ATTN J. NEMARICH, 13300
ATTN D. SCHAUBERT, 11500
ATTN CHIEF, 13000
ATTN F. CROWNE, 13200
ATTN R. LEAVITT, 13200 (10 COPIES)
ATTN C. MORRISON, 13200
ATTN J. SATTLER, 13200
ATTN G. SIMONIS, 13200
ATTN M. TOBIN, 13200
ATTN T. WORCHESKY, 13200
ATTN D. WORTMAN, 13200 (10 COPIES)
ATTN D. BARR, 13500
ATTN T. LISS, 15300
ATTN E. BROWN, 15400
ATTN S. KULPA, 15400
ATTN C. WILLETT, 15400
ATTN H. BRANDT, 22300
ATTN A. BROMBORSKY, 22300
ATTN J. SOLN, 22300
ATTN J. SILVERSTEIN, 22900
ATTN M. SOKOLOSKI, 00210
ATTN CHIEF, 13500
ATTN G. A. HUTTLIN, 22900
ATTN C. LANHAM, 00210
ATTN K. SANN, 11100
ATTN H. BRUNS, 15400
ATTN H. GERLACH, 11100
ATTN G. WALSH, 15300